Seismic coupling quantified on inferred décollements beneath the western syntaxis of the Himalaya

François Jouanne, Naveed Munawar, Jean-louis Mugnier, Awais Ahmed, Adnan Alam Awan, Pascale Bascou, Riccardo Vassallo

Seismic coupling quantified on inferred décollements beneath the western syntaxis of the Himalaya

François Jouanne (1), Naveed Munawar (2), Jean-Louis Mugnier (1), Awais Ahmed (2), Adnan Alam Awan (2), Pascale Bascou (1), Riccardo Vassallo (1).

(1) Université Grenoble Alpes, Université de Savoie-Mont-Blanc, CNRS, IRD, IFFSTAR, ISTerre F- 8 38041 Grenoble, France.
(2) Geoscience Advance Research Laboratories, Geological Survey of Pakistan, National Park Road, Chak Shahzad, Islamabad, Pakistan.

François Jouanne, Université Grenoble Alpes, Université de Savoie-Mont-Blanc, CNRS, IRD, IFFSTAR, ISTerre F- 8 38041 Grenoble, France. Francois.jouanne@univ-smb.fr

Naveed Munawar, Geoscience Advance Research Laboratories, Geological Survey of Pakistan, National Park Road, Chak Shahzad, Islamabad, Pakistan. ibnemunawar@gmail.com

Jean-Louis Mugnier, Université Grenoble Alpes, Université de Savoie-Mont-Blanc, CNRS, IRD, IFFSTAR, ISTerre F- 8 38041 Grenoble, France. Jean-Louis.Mugnier@univ-savoie.fr

Awais Ahmed Geoscience Advance Research Laboratories, Geological Survey of Pakistan, National Park Road, Chak Shahzad, Islamabad, Pakistan. muhammad.awais@ncp.edu.pk

Adnan Alam Awan, Geological Survey of Pakistan, Sariab Road, Quetta, Pakistan. adnan_gsp@yahoo.com

Pascale Bascou, Université Grenoble Alpes, Université de Savoie-Mont-Blanc, CNRS, IRD, IFFSTAR, ISTerre F- 8 38041 Grenoble, France. pascale.bascou@univ-smb.fr

Riccardo Vassallo, Université Grenoble Alpes, Université de Savoie-Mont-Blanc, CNRS, IRD, IFFSTAR, ISTerre F- 8 38041 Grenoble, France. Riccardo.Vassallo@univ-savoie.fr

Key points : interseismic deformation, Main Himalayen Thrust, GNSS

Abstract

We used episodic GNSS measurements to quantify the present-day velocity field in the northwestern Himalaya from the Himalayan foreland to the Karakoram Range. We report a progressive N-S compressional velocity gradient with two noticeable exceptions: in the Salt Range, where important southward velocities are recorded, and in Nanga Parbat, where an asymmetrical E-W velocity gradient is recorded. A review of Quaternary slip along active thrusts both in and out of sequence allows us to propose a 14 mm/year shortening rate. This

constraint, together with a geometrical model of the MHT, allows us to propose estimations of the slip distributions along the active faults. The lower flat of the MHT is characterized by ductile slip, whereas the coupling increases along the crustal ramp and along the upper flat of the MHT. The basal thrust of the Potwar Plateau and Salt Range presents weak coupling, which is interpreted as the existence of a massive salt layer forming an excellent décollement. In the central part of the frontal Salt Range, the velocities suggest the existence of a southward horizontal flux in the massive salt layer. The simulations also suggest that the velocities recorded in Nanga Parbat can be explained by active westward thrusting along the fault that borders the massif to the west. Simulations suggest that the slip along this fault evolves with depth from 5 mm/year ductile slip near the MHT to no slip along the upper part of the fault.

1. Introduction

The current deformation of the northwestern Himalaya appears distinctive compared to the deformation of the central Himalayas in several aspects: (1) the presence of the Potwar Plateau and the Salt Range, which are controlled by an excellent detachment level, (2) significant out-of-sequence deformation along the Balakot-Bagh or Riasi faults, and (3) the existence of the Nanga Parbat massif, interpreted as a crustal anticline and a crustal diapir (Khan et al., 2000; Sana, and Nath, 2016). To study the ongoing deformation in the northwestern Himalaya, we deployed a GPS network in northern Pakistan from the stable foreland south of the Salt Range to the Pakistan-China border. This network, measured in 2005, 2006, 2007, 2009, 2011-2012 and 2018-2019, made it possible to measure the velocity field and illustrate the interseismic and local postseismic deformation following the Balakot-Bagh earthquake in 2005. In this paper, we will go beyond the postseismic deformation to study, in detail, the interseismic deformation and coupling along the Main Himalayan Thrust. In this study, in addition to the velocities obtained from our network, we reanalyzed the available GPS data and included the published velocities for the Pir Panjal Range, Kashmir Valley and Ladakh.

Geological setting: geometry and quaternary slip rates of active faults in the northwestern Himalaya.

The present-day structure of the Himalayas is characterized by the underthrusting of the Indian lithosphere beneath the mountain chain along the Main Himalayan Thrust (MHT) (Zhao et al. 1993). This mountain chain absorbs approximately 14 to 21 mm yr−1 convergence, which is half of the convergence between India and Eurasia estimated by DeMets et al. (1994), depending on the location along the Himalayan arc. Large earthquakes of magnitude >8 affect

the MHT and have episodically ruptured segments several hundred kilometers long. In the western Himalaya, historical earthquakes (Bilham, 2019) and instrumental seismicity (Figs. 1 & 2) highlight the existence of a major seismic gap between the 2005 Balakot-Bagh earthquake and the 1905 Kangra earthquake (Fig. 1) and imply the existence of out-of-sequence deformation (the 2005 Mw 7.6 Balakot-Bagh earthquake), given that the thrust activated during this earthquake is located 100 km north of the MFT.

The structure of the western Himalaya also presents some particularities: (1) a frontal thrust (MFT) localized further south than in the rest of the Himalayas (Potwar Plateau and Salt Range), conditioned by the existence of a massive salt layer forming a particularly effective detachment plane, (2) a marked change in the structural direction from N80°W to N160-170°E (Figs. 1, 2, & 3), and (3) a crustal fold or diapir, the Nanga Parbat (Seeber and Armbruster., 1981; Seeber and Pêcher, 1998; Butler, 2018).

Potwar Plateau and Salt Range décollement

The northwestern Himalaya (Fig. 1) is characterized by regional-scale plateaus that mainly slip aseismically, as suggested by the lack of historical high-magnitude earthquakes (Fig. 2) in this area (Bilham et al., 2019). The largest of these plateaus is the Potwar Plateau, currently moving southwards above a late Precambrian-Early Cambrian salt layer that locally defines the MHT. Since 2 Ma, the propagation to the south of the MHT has reached this salt layer, which has enabled the Potwar Plateau to slip without frictional deformation. As a consequence, the emergence of the MHT along the Salt Range Thrust, the local expression of the Main Frontal Thrust, occurs to the south of this position in the Kashmir Himalaya, just east of the Potwar Plateau. On a geological time scale, the Potwar Plateau moves without internal deformation at 6 to 10.2 mm/year (Pennock et al., 1989; McDougall and Khan, 1990; McDougall et al., 1993; Grelaud et al., 2002; Mugnier et al., 2008, Cortes et al., 2017).

Main Frontal Thrust

To the east of the Salt Range, the frontal thrust is blind but marked by a well-expressed frontal anticline. The analysis of seismic profiles through this structure shows that the Main Frontal Thrust connects to the MHT at depths of 8-10 km. A thrust slip rate of 9+/- 3 mm/year has been estimated from an analysis of the deformed terraces carried by this frontal anticline (Vassallo et al., 2015).

Sinistral Jhelum strike-slip fault

The sinistral Jhelum strike-slip fault divides the region to the east with a structural orientation of N130° from the region to the west characterized by east-west-trending structures (Fig. 1). The continuity of this fault to the south means that it also forms the eastern boundary of the Potwar Plateau and Salt Range. This strike-slip fault delineates a domain characterized by an important deposit of salt during the Precambrian that led to the development of the Potwar Plateau and Salt Range and hence can be interpreted as a transfer fault between two domains with different distributions of deformation and tectonic styles.

Balakot–Bagh thrust and out-of-sequence thrusts

The Balakot–Bagh thrust is an active out-of-sequence thrust located 100 km north of the MFT, as shown by the occurrence of the Mw 7.6 8 October 2005 earthquake and its aftershocks (Bendick et al., 2007) (Fig. 3). The rupture of the 2005 earthquake affected a crustal ramp from its junction with the MHT at depth to the surface, as shown by studies of pixel displacements (Avouac et al., 2006; Yann et al., 2013). The postseismic deformation induced by this earthquake has been characterized by moderate afterslip occurring along the crustal ramp extending downdip from the rupture (Jouanne et al., 2011; Wang and Fialko, 2014). Trenching through the Balakot-Bagh thrust (Kondo et al., 2008) has documented the existence of large earthquakes along this fault. The coseismic slip of the 8 October 2005 earthquake and the dating of the previous event suggest that the Balakot-Bagh thrust absorbs ~3 mm/year of shortening.

This out-of-sequence thrust system continues eastward as the Medlicott-Wadia Thrust (MWT) (Thakur et al., 2010), located 20 km north of the frontal thrust. Morphotectonic analyses of the terraces deformed by thrusting (Vassallo et al., 2015; Vignon et al., 2016; Mugnier et al., 2017) have allowed the mean slip to be estimated at the Quaternary scale. Previous studies estimate that the MWT experiences localized deformation of 10 mm/year, while the frontal thrust absorbs shortening of 9+/- 3 mm/year (Vassallo et al., 2015).

Liachar brittle-ductile shear zone or Raikot-Liachar fault

The Liachar brittle-ductile shear zone (Butler & Prior, 1988; Butler, 2018), also known as the Raikot-Liachar fault (Madin et al., 1989), bounds the Nanga Parbat massif to the west with right-lateral strike and thrust components. The microseismicity associated with this fault makes it possible to determine a dip of 60° to the east. However, the lack of seismicity below 5 km suggests that the brittle-ductile boundary is situated at this depth (Meltzer et al. 2001).

Mukhopadhyay et al. 2011 proposed right-lateral focal mechanisms along the western boundary of the Nanga Parbat Massif and normal faulting in the central part of the massif.

2. Data acquisition and analysis

After the installation of a GNSS network dedicated to the quantification of postseismic deformation following the 8 October 2005 Kashmir earthquake (Jouanne et al., 2011), our preliminary GPS network was supplemented with points from the Karakoram Range to the Himalayan foreland south of the Salt Range and with points on either side of Nanga Parbat (Fig. 3). The remaining points of this large network were measured from October 2011 to February 2012 and again from October 2018 to February 2019 (Fig. 3 & Table 1). To complete this data set, available GPS data from UNAVCO measured between 2001 and 2010 (Khan et al., 2008; Ischuk et al. 2013) were also analyzed.

We analyzed data from episodic and permanent GNSS stations together with continuous GNSS network data from the GNSS sites defined in the ITRF2014 reference frame (ARTU, BADG, BAKU, BJFS, BJNM, CHUM, CUSV, GUAO, HYDE, IISC, IRKJ, IRKM, KIT3, KUWT, LHAZ, MDVJ, POL2, SGOC, SHAO, TALA, TASH, TCMS, TEHN, TNML, URUM, ZECK). Data were analyzed using Bernese 5.2 software (Dach et al., 2015) with absolute antenna phase center offset models in conjunction with precise orbits, Earth rotation parameters, and ocean tidal loading and atmospheric tidal loading estimates. Velocities and time series were estimated in the ITRF2014 reference frame (Altamimi et al., 2016) with discontinuities associate with this reference frame and expressed in terms of India-fixed reference frame (Fig. 3) by using the ITRF2014/India plate rotation pole proposed by Altamimi et al., 2017 (Table 2). To complete the data set in the Jammu-Kashmir area, we included data published by Kundu et al. 2014.

3. Results: Interseismic displacements at the surface

Throughout the rest of the Himalayas, during an interseismic period, the decollement is clearly locked to the Indian plate for 80% of its width along the Himalaya (Ader et al., 2012; Berger et al., 2003; Bettinelli et al., 2006; Jouanne et al., 1999; Jouanne et al., 2004; Kundu et al., 2014; Marechal et al. 2016, Stevens & Avouac, 2015; Jouanne et al., 2017, Dumka, 2018) whereas the Potwar and Kohat plateaus (Figs. 3 & 4) are creeping above a lubricated decollement to within 5 km of their frontal thrusts (Kahn et al 2011, Satyabala et al 2012).

By expressing the velocity field in the Nanga Parbat region with respect to a point to the west in the Kohistan Plateau (Fig. 5), the points located in Nanga Parbat have westward velocities reaching several millimeters per year with a very pronounced gradient. These observations suggest the existence of an active thrust within the Nanga Parbat Massif on the Kohistan Plateau along an inverted fault plunging eastward with a rather superficial locking depth. This inference is consistent with the distribution of microseismicity, few events of which occur at depth larger than 10 km; in addition, microseismicity tends to swarm along the Raikot-Liachar fault, an active fault that borders Nanga Parbat to the west (Meltzer et al. 2001). The velocity field is clearly not compatible with a symmetrical crustal diapir being deformed but corresponds instead to deformation along an inverted fault that would allow such a crustal diapir to flow westward.

2. Modeling interseismic displacements

Modeling the slip distributions along active faults requires knowledge of their geometries and, if possible, estimates of their maximum slip rates to add constraints during the inversion. The geometries of these faults can be known from geological sections; in the case of the MHT, its geometry can be inferred from the existence of a low-velocity zone that seems to be associated with this fault throughout the Himalayan arc. The maximum slip can be estimated from Quaternary slip rates along active faults while assuming that these slip rates reflect ductile slip rates along the deep parts of the faults.

Main Himalayan Thrust Geometry and Quaternary slip along the MHT.

The geometry of the Main Himalayan Thrust is, in conjunction with GNSS velocity measurements, key to estimating the locking of slip along the MHT and the detection of possible asperities. The MHT seems to be associated throughout the Himalayan arc with an area of low seismic wave velocities as revealed by receiver function analysis (Duputel et al., 2016). Recently published velocity profiles in the western Himalaya therefore make it possible to specify the major characteristics of this geometry. For northwestern Pakistan, Priestley et al, 2018 show a geometry for the MHT characterized by a long flat to the south with a northward dip of 3° at a depth of 10-12 km followed by a crustal ramp with a dip of approximately 15° below the greater Himalayas (Fig. 6). These characteristics of thick-skinned tectonism are also identified in the Jammu-Kashmir Himalaya, where the low-velocity zone associated with the MHT is found at depths of 12-16 km (Mir et al., 2017) below the Kashmir Valley, which is in

accordance with cross sections constructed for this area (Vassallo et al., 2015). The MHT would present as a crustal ramp to the north of the Kashmir Basin, where the Greater Himalaya region begins. East of the Kashmir Basin, microseismicity and source mechanisms (Paul et al., 2018) confirm this geometry with an MHT plunging northward by a few degrees to depths of 10-15 km. North of this crustal ramp, the MHT is probably flat with a plunge of a few degrees to the north (Fig. 6), as has been proposed for the Garhwal Himalaya (Pristley et al., 2018) or determined for the Nepal Himalaya (Berger et al., 2003; Jouanne et al., 2017). We suppose that the active out-of-sequence thrusts, the Balakot-Bagh thrust affected by the 8 October 2005 earthquake (Avouac et al., 2006; Pathier et al., 2006; Yan et al., 2013) and the Riasi fault or active Main Wadia Thrust (Vassallo et al., 2015; Vignon et al., 2016) are connected along the southern and upper flat of the MHT.

In the western extent of the study area, below the Potwar Plateau and Salt Range, the MHT is a decollement plane formed by a massive Precambrian salt layer (Butler et al., 1987; Jaume & Lillie, 1988). Seismic profiles and balanced cross sections (Pennock et al., 1989; Grelaud et al., 2002) allow us to characterize this part of the MHT as a decollement plane with a northward 3-5° dip reaching the surface in the Salt Range. The dextral strike-slip Kalabagh fault forms the western boundary of the Salt Range (Mcdougall & Khan, 1990; Chen & Khan, 2010; Khan et al., 2012).

We propose that these data be taken into account to consider an MHT geometry characterized by an upper flat with an upper boundary at a depth of 10 km, followed by a crustal ramp below the Higher Himalaya that is connected to a lower flat. This flat thrust follows the structural trend of the western Himalaya, as shown in Figure 1, which implies a drastic change in structural orientation between the Salt Range, where the faults and folds are oriented N80°, and the Jammu-Kashmir Himalaya, where the faults and folds are oriented N160-170° (Figs. 1, 2, 3 & 6). In the Salt Range and Potwar Plateau, the MHT extends southward; we have represented this part of the MHT as a plane reaching the surface that is connected at a depth of 10 km with the MHT north of the Potwar Plateau (Fig. 6).

Then, the slip along the MHT can be estimated as the sum of the slip along the Main Frontal Thrust (MHT near the surface) and of the slips along the out-of-sequence thrusts.

In the western part of the study area, the geological slip rate along the Salt Range (Fig. 1) can be estimated as being equal to the slip rate along the Kalabagh fault estimated at 7–10 mm/yr since 2 Ma (McDougall and Khan, 1990). Nevertheless, the observation of normal faults above the décollement may suggest that a part of the displacement along the décollement of the Salt

Range may be due to this N-S extension (Butler et al., 1987). At a distance of 170 km north of the Salt Range Thrust, the out-of-sequence Balakot-Bagh Thrust experienced a Mw 7.6 earthquake on 8 October 2005 (Kaneda et al., 2008) with coseismic slip localized along a crustal ramp dipping 30° between a depth of 15 km and the surface (Avouac et al., 2006; Pathier et al., 2006; Yan et al., 2013). Trenching through the Balakot-Bagh thrust (Kondo et al., 2008) has documented the occurrence of past large-scale earthquakes along this thrust. The coseismic slip of the 8 October 2005 earthquake and the dating of the previous event suggest that the Balakot-Bagh thrust absorbs ~3 mm/year of shortening. Accordingly, we can estimate the slip along the MHT to be 10 to 13 mm/year in the western part of the study area.

In the central part of the study area, at the junction between the Salt Range and the Jammu-Kashmir Himalaya, the analysis of deformed Quaternary terraces above the Mahesian anticline (Figs. 1, 2, & 3) and their dating results allow us to estimate a Quaternary uplift rate of 10.2+/-1.5 mm/year for the central part of this uplifted anticline (Cortés-Aranda et al., 2017). This uplift rate and geometry enable us to propose a shortening rate exceeding 10 mm/year across this fold for the Holocene. We can then estimate the Holocene slip rate along the MHT as the sum of this shortening rate and of the 3 mm/year shortening rate along the Balakot-Bagh Thrust.

In the eastern part of the study area, in the Jammu-Kashmir Himalaya (Figs. 1 & 2), the recent activity along the Medlicott-Wadia Thrust (MWT) has been investigated from geomorphic and tectonic perspectives (Vassallo et al., 2015; Vignon et al., 2016; Mugnier et al, 2017) and estimated at nearly 7.3 mm/yr (Mugnier et al, 2017). Accordingly, the analysis of the dated deformed terraces located on the frontal anticline carried by a blind thrust allows us to estimate a 9 +/- 3 mm/year shortening rate across this frontal fold (Vassallo et al. 2015).

If we consider these three estimations of the Quaternary slip rate along the MHT, we can adopt a value of ~14 mm/year. We can further assume that the Quaternary slip rate along the MHT and the ductile slip rate along the deeper part of the MHT are equivalent; we will then consider this value, 14 mm/year, both as the maximal slip along the MHT during the velocity inversion to determine the locking of slip and as the reference value to compute the coupling coefficient. This maximum slip is also close to the estimate of 13 mm/year by Jouanne et al. in 2013 for northern Pakistan and that of 13-14 mm/year from the GNSS network deployed in Jammu-Kashmir Himalaya and Ladakh (Kundu et al. 2014).

Jhelum strike-slip fault

We have considered that the Jhelum strike-slip fault (Fig. 1) is a vertical transfer fault separating the domain in the west with east-west-trending faults and folds from the domain in the east characterized by a NW-SE structural orientation. We suppose that this fault affects only the upper part of the crust above the Main Himalayan Thrust. Unfortunately, the lack of neotectonic investigations of the present-day slip along this fault means that we cannot constrain the maximum slip rate. The area south of the Jhelum fault where the folds change direction is affected by significant seismicity with earthquakes of magnitude greater than 5. Focal mechanisms (Fig. 4) show the existence of north-south shortening in the vicinity of the Mahesian anticline (Fig. 4), where neotectonic investigations (Cortes Aranda et al., 2017) have quantified a long-term shortening rate reaching 10 mm/year for the last 6.5 ka.

Raikot–Liachar fault.

The Raikot-Liachar fault, which borders the Nanga Parbat massif to the west, can be described as a nonrectilinear fault (Fig. 5) plunging 40° eastward according to the distribution of microseismicity. This fault places the metamorphic gneiss of Nanga Parbat over Quaternary sediments with a minimum displacement of 300 m (Owen, 1989); with the hypothesis that these sediments are 65,000 years old, the minimum thrust rate would be 4 mm/yr. This slip rate is a minimum, and we cannot use it to constrain the slip rate inversion using GNSS velocities; however, after the inversion, we can check whether the slip rates along the Raikot-Liachar fault are larger than or equal to 4 mm/year.

Slip distribution and coupling along the Main Himalayan Thrust, along the Nanga Parbat Thrust and the Jhelum strike-slip fault.

In our study, we did not use the back-slip approach (Savage 1983), but we have directly determined the slip on the fault using the SDM software (Wang et al., 2009, 2011, 2012). SDM (Steepest Descent Method) is a based on an iterative algorithm used for the constrained least-squares optimization. This software allows the use of curved faults that may have variations in dip, from which a set of rectangular segments is determined (~15*15 km in our study). This software allows the determination of an offset between the different datasets. This software requires a priori data such as the upper limit of the slip on the considered faults and the direction of the slip between a minimum and a maximum value (Table 3). The smooth slip model is realized through a smoothing term to be minimized with the misfit to data. In our study, the smoothing has been applied to slip and not to stress-drop, as possible, with a smoothing factor of 0.2.

During the inversion with sdm2011 software, we allow the slip rate along the MHT to reach up to 14 mm/year, which is supposed to be the maximum ductile slip rate at depth along the MHT (Figs. 8 & 9). We also allow a strike-slip component with the rake varying from -120° to -30° to take into account the obliquity of slip along the MHT due to the orientation of the thrust relative to the general interseismic velocities directed N190° in northwestern Himalaya. We use a low smoothing factor of 0.2 for the slip distribution to detect small-scale variations in the slip and coupling variations that may reflect the existence of asperities along the MHT. We also consider the decollement plane of the Potwar Plateau and Salt Range to be an active fault with a dip of 5° and dislocations that reach the surface, and we assume that a thrust allows the westward motion of Nanga Parbat above the Kohistan Plateau. For this last thrust, we use the distribution of microseismicity, which is apparently restricted to the top 5 km of the crust (Meltzer et al. 2001), to define a fault dipping 60° eastward. We suppose that this fault reaches the MHT at depth with a relatively low dip angle of 40°.

Our points in the area affected by postseismic deformation following the 8 October 2005 Balakot-Bagh earthquake (Jouanne et al., 2012) were destroyed before 2011, and thus, we were not able to estimate the linear and interseismic velocities for a time span after the end of postseismic deformation. We excluded the velocities during 2005-2007 within this zone from the study and ignored the Balakot-Bagh fault in our analysis of interseismic deformation. We also excluded the velocity at KERN published by Kundu et al., 2014, which was clearly affected by postseismic deformation. The residuals between the observed and simulated velocities (Fig. 7) are generally not significant, except those at points PS03, PS07, PS11 and PS16. These points are located in the Indus-Kohistan seismic zone within the geometrical extension of the Balakot-Bagh thrust (which was affected by the 8 October 2005 Mw 7.6 earthquake) in an area affected by large aftershocks subsequent to the main shock. The velocities at these points were determined with GNSS measurements (the first ones, which were recorded just after the earthquake in November 2005). We can then suppose that these velocities reflect the partial postseismic deformation following the Balakot-Bagh 2005 earthquake or its aftershocks. North of the network, near the China-Pakistan border, the points show significant residuals that can be interpreted as indicative of unmodeled velocities to the south. In this hypothesis, the residual velocities at the two points located north of the Main Karakoram Thrust could reveal the activity of this fault.

Our study uses data with a very disparate spatial distribution as shown in Figure 6. For example, it can be assumed that spatial coupling variations cannot be determined along the upper flat of the MHT in the western part of the study area, whereas such spatial variations can

probably be determined in the central and eastern part of the study area. To determine the impact of this unequal spatial distribution of the data, we used the bootstrap method (Efron and Tibshirani, 1986; Arnadottir and Segall, 1994, Hsu et al., 2003, Arnadottiret al., 2006; Serpelloni et al., 2010), which consists of randomly removing part of the data, in this case 10%, from the analysis, analysing the dataset thus constituted and repeating this a large number of times (200 in our study) to determine which parts of the model could be biased. To characterize the distribution of the solutions thus determined we estimated the standard deviation on the slip value for each patch (Fig. 10). As could be assumed, the western part of the model shows strong standard deviations (~ 3 mm/year) underlining that, in this region, the coupling is determined poorly, possible spatial variations in coupling cannot be determined, one can simply say that the upper flat of the MHT in the western part of the study area is probably locked.

The Salt Range thrust locally shows patches with standard deviations up to 2 mm/year (Fig. 10), we interpret these somewhat large standard deviations as reflecting insufficient data density to fully account for spatial variations in coupling along this thrust.

Similarly, further north, the Nanga Parbat thrust has patches with large standard deviations of up to 3 mm/year in its northern part, which underlines that the slip along the northern part of this fault is only constrained by the velocity of the point PK26, to solve this problem new points have been installed in 2019. The results of this study for the Jhelum Fault, on the contrary, show that the slip along this fault is well documented by the data.

We can compare also our coupling model with that of Li et al. 2018, which covers the same region as the region we are studying and which has considered some of the velocities previously published (Jouanne et al. 2012). These two models agree to determine a large blocked zone corresponding to the upper flat of the MHT, however the partial consideration of the published velocities for the Potwar Plateau and the Salt Range does not allow Li et al. 2018 to determine the coupling variations in this zone. Similarly, further north, the model of Li et al. 2018 presents a region with strong coupling at the level of the Indus - Kohistan Seismic Zone which exists in our model but in a less marked way.

6. Discussion

Main Himalayan Thrust

On the scale of the Potwar Plateau and the Salt Range (Fig. 4), the velocities show a north-south gradient. In contrast, the modeling results for the coupling along the MHT below the Potwar Plateau and Salt Range Thrust (Figs. 8 & 9) suggest local asperities and areas with low coupling. Analysis of the robustness of the coupling determination by the bootstrap method shows that at certain strong coupling variations (Fig. 8) patches with a high standard deviation (2 mm/year) are observed (Fig. 10). However, it should be noted that 2 mm/year corresponds to a standard deviation on the coupling of 0.14, a value which is much lower than the observed coupling variations reaching 0.4. We therefore assume that these strong coupling variations exist but that a higher measurement density would be needed to highlight them with more robustness.

We hypothesize that the Eocambrian salt layer (Fig. 11) induced low-coupling areas. We assume that the velocity field specific to this region (Fig. 4) reveals not only the tectonic origin of the region in the strictest sense but also a horizontal salt flow that affected the thick salt layers observed in the frontal and central parts of the Salt Range (points 0705, 0707, 1004, 2004, Awan, CNJP, and PM01). In the Salt Range, the present-day tectonism is therefore partly controlled by the horizontal flow of salt (Fig. 11) and by vertical flow along the Kalabagh fault, where diapirism is observed (Khan et al., 2012). We can therefore interpret the observation of normal faults in the front part of the Salt Range to represent the result of the subtraction of voluminous salt following this flow. Alternatively, could it be that fast slip in the past has shifted potential energy to the Salt Range that is currently manifest as high SW velocities as suggested by Cortés-Aranda et al., 2017.

To the north-west of the Potwar plateau the bootstrap method indicates that coupling variations cannot be detected because of the lack of data in this area. On the contrary, to the north-east of the Potwar Plateau, the coupling along the upper flat of the MHT presents a significant lateral variation (Figs. 8, 9 and 10). The salt layer may explain the lateral coupling variations along the upper flat of the MHT, to the northwest of the Potwar Plateau and in the vicinity of the Jhelum fault in the transition area between the Potwar Plateau and Jammu-Kashmir Himalaya, as reflected by the drastic change in structural orientation (Figs. 1 & 6). On the other hand, the coupling variations along the upper flat within the Kashmir Valley could indicate local fluctuations in the depth of the brittle-ductile transition along this upper flat within the depth range of 12-16 km (Vassallo et al., 2015; Mir et al., 2017). The spatial variation in the coupling along the upper flat of the MHT at equivalent depths may reflect lithological or thermal spatial variations.

The crustal ramp between the upper and lower flats of the MHT is affected by weak coupling along its eastern part to the north of Srinagar, while along its western part, in the area where coupling is well constrained, the ramp is in a coupled/uncoupled transition zone, i.e., the brittle-ductile transition zone. These variations may reflect lithological or thermal variations along the MHT.

North of the crustal ramp, coupling along the lower flat is absent (Figs. 8 & 9), which suggests the existence of ductile deformation along the lower flat, as observed, for example, in Nepal (Ader et al., 2012; Berger et al., 2003; Bettinelli et al., 2006; Jouanne et al., 1999; Jouanne et al., 2004; Jouanne et al., 2017; Stevens & Avouac, 2015). It must be underlined that the coupling increase determined in the north-western part of our study area along the lower flat of the MHT (Fig. 8) corresponds at an area where the bootstrap method indicates that the coupling is poorly constrained (Fig. 10), we can then suppose that this coupling variation has not necessary a geological meaning.

The approximate location of historical earthquakes indicates that they are generally located in areas with strong coupling variations, either near the crustal ramp or at the upper flat of the MHT. The presence of historic earthquakes at the lower ductile MHT flat could correspond to extensional earthquakes as suggested by the focal mechanisms in this region (Fig. 2) indicating an E-W extension.

Jhelum strike-slip fault

The role of the Jhelum strike-slip fault in the transition between the structural orientation of the Salt Range (N80°) and that of the Jammu-Kashmir Himalaya (N150°) is unclear. If we consider this fault in the numerical simulation of the current displacement field, assuming that it extends from the surface to the MHT, then a dextral strike-slip rate of up to 6 mm/year is determined from the surface to its connection with the MHT (Fig. 9). However, the numerical simulation of the slip along the dextral Jhelum strike-slip fault does not show any variation with depth. The upper part of the fault does not appear to be locked. This behavior could be related to the observation of serpentine bodies along the fault zone that would allow the existence of creep, even near the surface. Nevertheless, a denser GNSS network than that used herein would be necessary to better constrain the distribution of slip over this fault although analysis of the reliability of the slip on this fault by the bootstrap method shows that this estimate is robust (Fig. 10).

Indus Kohistan Seismic Zone

Microseismicity, the Patan earthquake in 1974 and the aftershocks following the Balakot Bagh earthquake (MonaLisa et al. 2009) help to define this zone characterized by a seismicity swarm. This zone can be interpreted as the north-westward propagation of the Balakot-Bagh fault, site of the 2005 earthquake (Jouanne et al., 2011). The location of this zone on the coupling map shows that this zone also corresponds to a zone where strong coupling variations exist. We can thus propose that the abrupt change of coupling induces a local increase of deviation stress associated with this seismicity swarm.

Liachar brittle-ductile shear zone or Raikot-Liachar fault (Figs. 5, 9 & 12).

The velocity field expressed with respect to a point located in Kohistan shows asymmetric velocities to the west in the Nanga Parbat massif (Fig. 5). The velocities were numerically simulated considering the geometry of the reverse and strike-slip fault that borders this massif to the west (Fig. 12). The simulated fault slips along the central part of this boundary fault decrease from 5 mm/year at depth to a fraction of a millimeter per year near the surface. We interpret this evolution as a reflection of the change in the deformation regime from ductile deformation at depth to brittle deformation, marked by a swarm of microseismicity at relatively shallow depth. We can notice good agreement between the distribution of microseismicity and the upper part of the fault that is almost blocked, as shown by the numerical simulation of velocities (Fig. 12), and good agreement is also observed with the Quaternary slip along the fault estimated at ~4 mm/year.

Hazard implications.

The estimation of the seismic alea of the eastern part of the study area, Jammu and Kashmir, can be based on fairly detailed historical seismicity (Bilham et al., 2019) and paleoseismological studies along the Riasi out-of-sequence thrust, which is not possible along the MFT, which is blind here. The last major earthquakes in Kashmir were the 1555 earthquake (Mw 7.6 to 8) and the 2005 Mw 7.6 earthquake. We join by Schiffman et al. 2013 in pointing out that the MHT in this region is largely locked (Fig. 8). As the last earthquake probably affected this segment, at least partially dating from 1555, we can conclude like Bilham et al.,

2017, 2019 that this segment of the Himalayan chain is sufficiently mature to be affected by a strong earthquake of magnitude (Mw > 8) and that earthquakes of very strong magnitudes (Mw ~9) must occur from time to time to release the entire slip deficit.

The estimation of the seismic alea of northern Pakistan is difficult due to the absence of a major historical reference earthquake, with the possible exception of the Taxila earthquake in 25 AD (Ambraseys et al., 1975), and the absence of a paleoseismological calendar. The paleoseismological calendar is only known for the Balakot-Bagh thrust (Kondo et al. 2008) but not for the MFT at the Salt Range. It can indeed be assumed that a very strong magnitude earthquake along the MHT would not propagate in the salt level forming the detachment of the Potwar Plateau and the Salt Range, but would induce a strong post-seismic deformation controlled by the rheology of the salt. It can therefore be assumed that the postseismic deformation would not be sufficiently localized to be studied by neotectonic methods, by trenching the Salt Range Thrust - MFT for example.

On the other hand, with our study we can quantify the surface likely to be affected by a very strong magnitude earthquake, this surface corresponds to the sum of the MHT patches corresponding to northern Pakistan presenting a non-zero coupling. Assuming that the previous large magnitude earthquake, the hypothetical Taxila AD 25 earthquake by example, released all the previously accumulated slip deficit and that the future earthquake will release all the slip deficit accumulated since the last very large earthquake, then assuming that the geodetic coupling has not changed over time, we can use the sum of the seismic moments calculated with our model to propose a Mw magnitude. We can then propose that in the area covered by our study a Mw of 8.8 earthquake could occurred each 2000 years, a Mw 8.6 earthquake each 1000 years or a Mw 8.4 each 500 years if all the patches break during a single earthquake and if we neglect the afterslip which could release part of the slip deficit probably in the deep part of the MHT.

If we assume that the afterslip releases a seismic moment equivalent to 34.0% of the co-seismic moment as proposed by Gualandi et al, 2017 for the 2015 Gorkha earthquake in Nepal, we can correct the above estimates, with an earthquake of Mw 8.69 every 2000 years, an earthquake of Mw 8.49 every 1000 years and an earthquake of Mw 8.28 every 500 years.

If now we consider that a single earthquake can affect not only Northern Pakistan but also Kashmir we can propose with our slip distribution, if we assume that all the slip deficit accumulated before the 1555 earthquake was released in that earthquake, a magnitude Mw 8.63

if Northern Pakistan is affected by an earthquake every 500 years, a magnitude Mw 8.74 if an earthquake occurs every 1000 years in Northern Pakistan and a magnitude Mw 8.88 if it occurs every 2000 years. If, as before, we assume the existence of an afterslip that releases 34% of the seismic moment, we can correct the above estimates, with an earthquake of Mw 8.51 every 500 years, an earthquake of Mw 8.62 every 1000 years and an earthquake of Mw 8.76 every 2000 years.

We can reasonably assume that from the 16th century onwards, there are no major earthquakes not reported in historical sources in northern Pakistan, we can therefore assume that this region may be affected by a major earthquake with a moment magnitude Mw greater than 8.3 (or 8.63 if Kashmir is also affected) if all the slip deficit is released, which could reach Mw 8.7 if the last very strong earthquake occurred 2000 years ago in northern Pakistan. Earthquakes of such very strong magnitudes are reported in the Himalayas, we can thus note for example the following earthquakes: 1100 ± 50 Mw 9 event which is not associated with historical sources in the eastern Himalayas (Wesnousky et al. 2019), 1225 Mw 7.5- 8.5 Nepal (Pant 2002, Sapkota et al. 2013), 1400 ± 50 Mw 8.0- 8.5 in Western Himalaya (Kumar et al. 2001, 2006), 1505 Mw 8.2 - 8.9 eastern Nepal and Kumaon (Jackson 2000; Ambraseys & Jackson 2003), the 1934 Bihar Nepal earthquake Mw 8.4 (Chen & Molnar 1977, 1983) and the 1950 Assam earthquake Mw 8.7 (Chen & Molnar 1977).

Conclusion

Measurements of the velocity field in the northwestern Himalaya revealed coupling variations along the basal overlap of the Potwar Plateau and Salt Range that could be related to variations in the thickness of the salt layer forming the detachment plane. In the central part of the Salt Range, the measured horizontal velocities suggest the existence of very significant horizontal creep of the very thick salt layer at this location, while along the Kalabagh fault, salt diapirism is observed. The Jhelum fault separating the Potwar Plateau, which is characterized by a thick layer of salt, from the rest of the Himalayas is a dextral strike-slip fault affected by creep of 6 mm/year. Along the upper flat of the MHT, the coupling evolves from full to weak coupling, which may or may not be weak at the level of the crustal ramp separating the upper flat from the lower flat of the MHT. The lower flat of the MHT is characterized by no coupling, suggesting the existence of ductile deformation along the MHT. The absence of recent earthquakes of very high magnitude in the historical seismicity and coupling along the MHT determined by our study suggests that earthquakes of very high magnitudes (Mw > 8) could

affect northern Pakistan. Finally, our simulation of the velocity field suggests that the current deformation of Nanga Parbat is mainly controlled by its westward thrusting over the Kohistan Plateau. The estimated slips along the Nanga Parbat Thrust show slips reaching 6 mm/year at depth, and the slip gradually decreases until it is almost absent along the upper part of the fault, which is probably brittle, as is indicated by a swarm of microseismicity.

Acknowledgments

The authors would like to thank R. Bilham, the Associate Editor L. Dal Zilio, and three anonymous reviewers for their insightful remarks. The figures and maps were prepared using Generic Mapping Tools software (Wessel and Smith, 1995) and Paraview software (Ahrens et al., 2005; Ayachit, 2015). This material is partially based on data provided by UNAVCO with support from the National Science Foundation (NSF) and the National Aeronautics and Space Administration (NASA) under NSF Cooperative Agreement No. EAR-0735156, United States. Funding was also provided by INSU-CNRS, France, and the AAP of Savoie Mont Blanc University, France. After acceptance of this paper, data used in this study will be place in a repository.

References

Ader, T., Avouac, J.P., Liu-Zeng, J., Lyon-Caen, H., Bollinger, L., Galetzka, J., Genrich, J., Thomas, M., Chanard, K., Sapkota, S., Rajaure, S., Shrestha, P., Ding, L., Flouzat, M., 2012. Convergence rate across the Nepal Himalaya and interseismic coupling on the Main Himalayan Thrust: implications. J. Geophys. Res. 117, B04403. http://dx.doi.org/10.1029/2011JB009071.

Ahrens, J., Geveci, B., Law, C., 2005. ParaView: An End-User Tool for Large Data Visualization, Visualization Handbook. Elsevier ISBN-13: 978-0123875822.

Altamimi, Z., Rebischung, P., Métivier, L., Xavier, C., 2016. ITRF2014: A new release of the International Terrestrial Reference Frame modeling nonlinear station motions, *J. Geophys. Res. Solid Earth*, 121, doi:10.1002/2016JB013098.

Altamimi, Z., L. Métivier, P. Rebischung, H. Rouby and X. Collilieux (2017) ITRF2014 Plate Motion Model, *Geophysical Journal International*, vol. 209, n. 3, pp. 1906--1912, doi:10.1093/gji/ggx136.

Ambraseys, N., Lensen, G., Moinfar, M., 1975. The Pattan Earthquake of 28 Dec., 1974. Reconnaissance Report Prepared for the Government of Pakistan and UNESCO. Paris.

574 Ambraseys N. & Jackson, D. 2003. A note on early earthquakes in northern India and
575 southern Tibet. Current Science, 84, 570–582.
576 Arnadottir, T., and P. Segall (1994), The 1989 Loma Prieta earthquake imaged from
577 inversion of geodetic data, J. Geophys. Res., 99, 21,835–21,855.
578 Arnadottir, T., W. Jiang, K. L. Feigl, H. Geirsson, and E. Sturkell (2006), Kinematic
579 models of plate boundary deformation in southwest Iceland derived from GPS observations, J.
580 Geophys. Res., 111, B07402, doi:10.1029/2005JB003907.
581 Avouac, J.-P., Ayoub, F., Leprince, S., Konca, O., and Helmberger, D., 2006, The 2005
582 Mw 7.6 Kashmir earthquake: sub-pixel correlation of ASTER images and seismic waveform
583 analysis, Earth Planet. Sci. Lett. 249, 514-528.
584 Ayachit, U., 2015. The ParaView Guide: A Parallel Visualization Application. Kitware
585 ISBN 978-1930934306.
586 Baker, D.M., Lillie, R.J., Yeats, R.S., Johnson, G.D., Yousuf, M., Zamin, A.S.H., 1988.
587 Development of the Himalayan frontal thrust zone: salt Range, Pakistan. Geology 16, 3e7.
588 http://dx.doi.org/10.1130/0091-7613(1988)016<0003: DOTHFT>2.3.CO;2.
589 Bendick, R., R. Bilham, M. Asif Khan, and S. Faisal Khan (2007), Slip on an active
590 wedge thrust from geodetic observations of the 8 October 2005 Kashmir earthquake, Geology,
591 35, 267–270, doi:10.1130/G23158A.1.
592 Berger, A., Jouanne, F., Hassani, R., Mugnier, J.L., 2003. Modelling the spatial
593 distribution of present-day deformation in Nepal. How cyclindrical is the Main Himalayan
594 Thrust in Nepal? Geoph. J. Int. 156 (1), 94e112.
595 Bettinelli P., Avouac J.P., Flouzat M., Willis P., Jouanne F., Bollinger L., Chitrakar
596 G.R., (2006), Interseismic deformation in the Himalaya of Central Nepal from combined GPS
597 measurements and DORIS data, Journal of Geodesy.
598 Bilham, R., Mencin, D., Bendick, R. & Bürgmann, R., (2017). Implications for elastic
599 energy storage in the Himalaya from the Gorkha 2015 earthquake and other incomplete ruptures
600 of the Main Himalayan Thrust. Quaternary International, 462, 3–21,
601 https://doi.org/10.1016/j.quaint.2016.09.055.
602 Bilham, R. (2019), Past and future Himalayan earthquakes: a 2018 estimate of slip
603 potential based on the past five centuries of historical seismicity, in Treloar, P. J. & Searle, M.
604 P. (eds) Himalayan Tectonics: A Modern Synthesis.. *Geological Society, London, Special*
605 *Publications* Version: 1, doi: 483, 1-61.

606 Butler, R.W., Coward, M.P., Harwood, G.M., Knipe, R.J., 1987. Salt control on thrust
607 geometry, structural style and gravitational collapse along the Himalayan mountain front in the
608 Salt Range of northern Pakistan. Dyn. Geol. Salt Relat. Struct. 399e418.
609 Butler, R.W.H. & Prior, D.J. 1988. Tectonic controls on the uplift of Nanga Parbat,
610 Pakistan Himalayas. Nature, 333, 247–250.
611 Butler, R.W., 2018. Tectonic evolution of the Himalayan syntaxes: the view from Nanga
612 Parbat.Geological Society, London, Special Publications, 483, 30, August 2018,
613 htpps://doi.org/10.1144/SP483.5.
614 Chen, W., Molnar, P., 1977. Seismic moments of major earthquakes and the average
615 rate of slip in central Asia. J. Geophys. Res. 82, 2945–2969.
616 Chen, W.P. & Molnar, P. 1983. Focal depths of intracontinental and intraplate
617 earthquakes and their implications for the thermal and mechanical properties of the lithosphere.
618 J. Geophys. Res. Solid Earth, 88, 4183–4214.
619 Chen, L., Khan, S.D., 2010. InSAR observation of the strike-slip faults in the northwest
620 Himalayan frontal thrust system. Geosphere 6, 731e736.
621 http://dx.doi.org/10.1130/GES00518.1.
622 Cortés-Aranda J., Mugnier J.L., Jouanne F., Vassallo R.**,** Carcaillet J., Alam A.A., 2017.
623 Holocene shortening rates and seismic hazard assessment for the frontal Potwar Plateau, NW
624 Himalaya of Pakistan : Insights from 10Be concentrations on fluvial terraces in the Mahesian
625 Anticline. Quaternary International, 462, 75-9. http://dx.doi.org/10.1016/j.quaint.2017.02.032.
626 Dach, R., S. Lutz, P. Walser, P. Fridez (Eds); 2015: Bernese GNSS Software Version
627 5.2. User manual, Astronomical Institute, University of Bern, Bern Open Publishing.
628 DOI: 10.7892/boris.72297; ISBN: 978-3-906813-05-9.
629 DeMets, C., Gordon, R.G., Argus D.F & Stein S., 1994. Effect of recent revisions to the
630 geomagnetic reversal time scale on estimates of current plate motions. *Geophys. Res. Lett.*, **21,**
631 2191–2194.
632 Dziewonski, A. M., T.-A. Chou and J. H. Woodhouse, Determination of earthquake
633 source parameters from waveform data for studies of global and regional seismicity, J.
634 Geophys. Res., 86, 2825-2852, 1981. doi:10.1029/JB086iB04p02825
635 Dumka R. K., Kotlia B., Kothyari G. Ch., Paikrey J. Dimri S., (2018), Detection of
636 high and moderate crustal strain zones in Uttarakhand Himalaya, India, Acta Geodaetica et
637 Geophysica 53(B11), DOI: 10.1007/s40328-018-0226-z.

Duputel, Z., Vergne, J., Rivera, L., Wittlinger, G., Farra, V., Hetényi, G., 2016. The 2015 Gorkha earthquake: a large event illuminating the Main Himalayan Thrust fault. Geophys. Res. Lett. 43 (2517–2525), 2016G. http://dx.doi.org/10.1002/L068083.

Efron, B., and R. Tibshirani (1986), Bootstrap methods for standard errors, confidence intervals, and other measures of statistical accuracy, Stat. Sci., 1, 54– 77.

Ekström, G., M. Nettles, and A. M. Dziewonski, The global CMT project 2004-2010: Centroid-moment tensors for 13,017 earthquakes, Phys. Earth Planet. Inter., 200-201, 1-9, 2012. doi:10.1016/j.pepi.201204.002.

Gualandi, Adriano and Avouac, Jean-Philippe and Galetzka, John and Genrich, Joachim F. and Blewitt, Geoffrey and Adhikari, Lok Bijaya and Koirala, Bharat Prasad and Gupta, Ratnamani and Upreti, Bishal Nath and Pratt-Sitaula, Beth and Liu-Zeng, Jing (2017) *Pre- and post-seismic deformation related to the 2015, M_w 7.8 Gorkha earthquake, Nepal*. Tectonophysics, 714-715. pp. 90-106. ISSN 0040-1951.

Grelaud, S., Sassi, W., de Lamotte, D.F., Jaswal, T., Roure, F., 2002. Kinematics of eastern salt Range and south Potwar basin (Pakistan): a new scenario. Mar. Pet. Geol. 19, 1127e1139. http://dx.doi.org/10.1016/S0264-8172(02)00121-6.

Hsu, Y.-J., M. Simons, S.-B. Yu, L.-C. Kuo, and H.-Y. Chen (2003), A two dimensional dislocation model for interseismic deformation of the Taiwan mountain belt, Earth Planet. Sci. Lett., 211, 287 – 294.

Ischuk, A., et al. (2013), Kinematics of the Pamir and Hindu Kush regions from GPS geodesy, J. Geophys. Res. Solid Earth, 118, 2408–2416, doi:10.1002/jgrb.50185.

Jackson, D. 2000. The great Himalayan earthquake of 1505: Rupture of the Central Himalayan Gap? In: BLEZER, H. (ed.) Tibet, Past and Present: Tibetan Studies 1. PIATS 2000: Tibetan Studies : Proceedings of the Ninth Seminar of the International Association for Tibetan Studies, Leiden 2000. Brill, Boston, MA, 147–153.

Jaume, S.C., Lillie, R., 1988. Mechanics of the Salt Range-Potwar Plateau, Pakistan: a fold and thrust belt underlain by evaporates. Tectonics 7, 57e71.

Jouanne, F., Mugnier, J.L., Pandey, M.R., Gamond, J.F., Le Fort, P., Serrurier, L., Vigny, C., Avouac, J.P. & IDYLHIM members (1999). - Oblique convergence in the Himalayas of western Nepal deduced from preliminary results of GPS measurements. Geoph. Res. Lett. N°13, V.26, p. 1933-1936.

Jouanne F., Mugnier J. L., Gamond J. F., Le Fort P., Pandey M.R., Bollinger L., Flouzat M., Avouac J.P., (2004), Current shortening across the Himalayas of Nepal, Geophys. J. Int.,157, 1-14.

672 Jouanne, F., Awan, A., P^echer, A., Kausar, A., Mugnier, J.L., Khan, I., Khan, N.A.,
673 Van Melle, J., 2014. Present-day deformation of northern Pakistan from salt ranges to
674 Karakorum ranges. J. Geophys. Res. Solid Earth 119, 2487e2503.
675 http://dx.doi.org/10.1002/2013JB010776.
676 Jouanne, F., Awan, A., Madji, A., Pêcher, A., Latif, M., Kausar, A., Mugnier, J.L.,
677 Khan, I., Khan, N.A., 2011. Postseismic deformation in Pakistan after the 8 October 2005
678 earthquake: evidence of afterslip along a flat north of the Balakot-Bagh Thrust. *J. Geophys.*
679 *Res.*, 116, B07401, doi:10.1029/2010JB007903.
680 Jouanne F., Mugnier J.L., Sapkota S.N., Bascou B., Pecher A., 2017. Estimation of
681 coupling along the Main Himalayan Thrust in the central Himalaya. *Journal of Asian Earth*
682 *Sciences*, January 2017.
683 Kaneda, H., T. Nakata, H. Tsutsumi, H. Kondo, N. Sugito, Y. Awata, S. S. Akhtar, A.
684 Majid, W. Khattak, A. A. Awan, R. S. Yeats, A. Hussain, M. Ashraf, S. G. Wesnousky, and A.
685 B. Kausar (2008), Surface rupture of the 2005 Kashmir, Pakistan, earthquake, and its active
686 tectonic implications, *Bull. Seismol. Soc. Am.*, 98, 521–
687 557. https://doi.org/10.1785/0120070073.
688 Khan, M.A., Treloar, P.J., Searle, M.P., and Jan, M.Q., (eds) 2000. Tectonics of the
689 Nanga Parbat Syntaxis and the Western Himalaya. Geological Society, London, Special
690 Publication, v.170, pp: 2
691 Khan, M. A., R. Bendick, I.M. Bhat, R. Bilham, D.M. Kakar. S. F. Khan, S. H. Lodi,
692 M. S. Qazi, B. Singh, W. Szeliga amd A. Wahab, 2008. Preliminary geodetic constraints on
693 plate boundary deformation on the western edge of the Indian Plate from TriGGNnet, *J.*
694 *Himalayan Earth Sciences*, 41 (2008), 71-87). Peshawar 2010.
695 Khan, S.D., Chen, L., Ahmad, S., Ahmad, I., Ali, F., 2012. Lateral structural variation
696 along the Kalabagh Fault Zone, NW Himalayan foreland fold-and-thrust belt, Pakistan. J. Asian
697 Earth Sci. 50, 79e87. http://dx.doi.org/10.1016/j.jseaes.2012.01.009.
698 Kondo, H., Nakata, T., Akhtar, S.,Wesnousky, S., Sugito, N., Kaneda, H., Tsutsumi, H., Khan,
699 A., Khattak,W., Kausar, A., (2008). Long recurrence interval of faulting beyond the 2005
700 Kashmir earthquake around the northwestern margin of the Indo-Asian collisionzone. Geology
701 36, 731–734. http://dx.doi.org/10.1130/G25028A.
702 Kumar S, Wesnousky WG, Rockwell TK, Ragona D, Thakur VC, Seitz GG (2001)
703 Earthquake recurrence and rupture dynamics of Himalayan Frontal Thrust, India. Science
704 294:2328–2331.

Kumar, S., Wesnousky, S., Rockwell, T.K., Briggs, R.W., Thakur, V.C., Jayangondaperumal, R., 2006. Paleoseismic evidence of great surface rupture earthquakes along the Indian Himalaya. J. of Geophysical Res. 111, B03304. doi:10.1029/2004JB003309.

Kundu, B., R. K. Yadav, B. S. Bali, S. Chowdhury, and V. K. Gahalaut (2014), Oblique convergence and slip partitioning in the NW Himalaya: Implications from GPS measurements, Tectonics, 33, 2013–2024, doi:10.1002/2014TC003633.

Li, S., Wang, Q., Yang, S., Qiao, X., Nie, Z., Zou, R., et al. (2018). Geodetic imaging mega-thrust coupling beneath the Himalaya. Tectonophysics 747, DOI: 10.1016/j.tecto.2018.08.014.

McDougall, J.W., Hussain, A., Yeats, R.S., 1993. The Main Boundary Thrust and propagation of deformation into the foreland fold-and-thrust belt in northern Pakistan near the Indus River. Geol. Soc. Lond. Spec. Publ. 74, 581e588.

Mcdougall, J.W., Khan, S.H., 1990. Strike-slip faulting in a foreland foldthrust belt: the Kalabagh Fault and western salt Range, Pakistan. Tectonics 9, 1061e1075.

Madin, I.P., Lawrence, R.D. & Ur-Rehman, S, 1989. The northwestern Nanga Parbat-Haramosh massif; evidence for crustal uplift of the northwestern corner of the Indian craton. In: MALINCONICO, L.L. & LILLIE, R.J. (eds) Tectonics of the Western Himalayas. Geological Society of America, Special Papers, 232, 169–182.

Marechal A., Mazzotti S., Cattin R., Cazes G, Vernant P., Drukpa D., Thinley K., Tarayoun A., Le Roux-Mallouf R., Thapa B. B., et al.. Evidence of interseismic coupling variations along the Bhutan Himalayan arc from new GPS data. Geophysical Research Letters, American Geophysical Union, 2016, 43 (24), pp.12399-12406. ff10.1002/2016GL071163ff. ffhal-01689807.

Meltzer, A., G. Sarker, B. Beaudoin, L. Seeber, and J. Armbruster (2001), Seismic characterization of an active metamorphic massif, Nanga Parbat, Pakistan, Himalayan Geol., 29, 651 – 654, doi:10.1130/0091-7613.

Mir RR, Parvez IA, Gaur VK, Chandra R, Romshoo SA, 2017, Crustal structure beneath the Kashmir Basin adjoining the western Himalayan syntaxis, Bulletin of the Seismological Society of America 107 (5), 2443-2458.

Mona Lisa, Khwaja, A.A., Jan, M.Q. *et al.* (2009). New data on the Indus Kohistan seismic zone and its extension into the Hazara–Kashmir Syntaxis, NW Himalayas of Pakistan. *J Seismol* **13,** 339–361. https://doi.org/10.1007/s10950-008-9117-z

Mukhopadhyay, Basab , Acharyya, Anshuman , Bhattacharyya, Debkumar , Dasgupta, Sujit and Pande, Prabhas (2011) 'Seismotectonics at the terminal ends of the Himalayan Arc', Geomatics, Natural Hazards and Risk, 2: 2, 159 — 181.

Mugnier, J.-L., Vignon V. , Jayangondaperumal R. , Vassallo R., Malik M.A., Replumaz A., Srivastava R.P. , Jouanne F., Buoncristiani J.F., Jomard H., Carcaillet J., (2017) A complex thrust sequence in western Himalaya: The active Medlicott Wadia Thrust, Quaternary International, http://dx.doi.org/10.1016/j.quaint.2017.05.028.

Owen, L. A. (1989), Neotectonics and glacial deformation in the Karakoram Mountains and Nanga Parbat Himalaya, Tectonophysics, 163, 227–265.

Pant, M.R. 2002. A step toward a historical seismicity of Nepal. Adarsa, 2, 29–60.

Pathier, E., Fielding, E., Wright, T., Walker, R., Parsons, B., and Hensley, S., 2006, Displacement field and slip distribution of the 2005 Kashmir earthquake from SAR imagery, Geophys. Res. Lett. 33, L20310.

Paul, H., Priestley, K. F., Powali, D., Sharma, S., Mitra, S., & Wanchoo, S. K. (2018). Signatures of the existence of frontal and lateral ramp structures near the Kishtwar Window of the Jammu and Kashmir Himalaya: Evidence from microseismicity and source mechanisms. *Geochemistry, Geophysics, Geosystems, 19,* 3097–3114. https://doi.org/10.1029/2018GC007597.

Pennock, E.S., Lillie, R.J., Zaman, A.S.H., Yousuf, M., 1989. Structural interpretation of seismic reflection data from eastern Salt Range and Potwar Plateau. Pak. Am.Assoc. Pet. Geol. Bull. 73, 841e857.

Sana, H., and Nath., S.K. 2016. In and around the Hazara-Kashmir syntaxis: a seismotectonic and seismic hazard perspective, J. Ind. Geophys. Union (September 2016) v.20, no.5, pp: 496-505.

Sapkota, S., Bollinger, L., Klinger, Y., Tapponnier, P., Gaudemer, Y., Tiwari, D., 2013. Primary surface ruptures of the great Himalayan earthquakes in 1934 and 1255. Nat. Geosci. 6, 71–76. http://dx.doi.org/10.1038/ngeo1669.

Satyabala, SP, ZH Yang and R Bilham (2012), Stick-slip advance of the Kohat Plateau in Pakistan. *Nat. Geosci.* Version: 1 *5* (2) 147-150, issn: 1752-0894, ids: 893ZU, doi: 10.1038/NGEO1373.

Savage J.C., 1983. A dislocation model of strain accumulation and release at a subduction zone, *J. geophys. Res.*, 88, 4984–4996. https://doi.org/10.1029/JB088iB06p04984.

Schiffman, C., Bali, B.S., Szeliga, W., Bilham, R., 2013. Seismic slip deficit in the Kashmir Himalaya from GPS observations. Geophys. Res. Lett. 40, 5642–5645.

771 Seeber, L., Armbruster, J.G., 1981. Great detachment earthquakes along the Himalayan
772 Arc and long-term forecasting. In: Sibson, D.W., Richards, P.G. (Eds.), Earthquake Prediction:
773 An international review. American Geophysical Union. Maurice Ewing Series, 4, Amer.
774 Geophysical Union, pp. 259e277. http://dx.doi.org/10.1029/ME004p0259.
775 Seeber, L., and A. Pêcher (1998), Strain partitioning along the Himalayan arc and the
776 Nanga Parbat antiform, Geology, 26, 791 – 794, doi:10.1130/0091-7613(1998)026.
777 Serpelloni, E., R. Burgmann, M. Anzidei, P. Baldi, B. Mastrolembo Ventura, and E.
778 Boschi (2010), Strain accumulation across the Messina € Straits and kinematics of Sicily and
779 Calabria from GPS data and dislocation modeling, Earth Planet. Sci. Lett., 298(3–4), 347–360,
780 doi: 10.1016/j.epsl.2010.08.005.
781 Stevens, V. L., and J. P. Avouac (2015), Interseismic coupling on the main Himalayan
782 thrust, Geophys. Res. Lett., 42, 5828–5837, doi:10.1002/2015GL064845.
783 Thakur, V.C., Jayangondaperumal, R., Malik, M.A., 2010. Redefining Medlicott-
784 Wadia's main boundary fault from Jhelum to Yamuna, an active fault strand of the main
785 boundary thrust in northwest Himalaya. Tectonophysics 489, 29–42.
786 Vassallo, R., Mugnier, J.-L., Vignon, V., Malik, M. a., Jayangondaperumal, R.,
787 Srivastava, P., Jouanne, F., Carcaillet, J., 2015. Distribution of the late-quaternary deformation
788 in northwestern Himalaya. Earth Planet. Sci. Lett. 411, 241e252.
789 http://dx.doi.org/10.1016/j.epsl.2014.11.030.
790 Vignon V, Mugnier J-L, Vassallo R, Srivastava P, Malik MA, Jayangondaperumal R,
791 Jouanne F, Buoncristiani JF, Carcaillet J, Replumaz A, Jomard H, (2016). Sedimentation close
792 to the active Medlicott Wadia Thrust (Western Himalaya) : How to estimate climatic base level
793 changes and tectonics, Geomorphology, http://dx.doi.org/10.1016/j.geomorph.2016.07.040.
794 Wang, L., Wang, R., Roth, F., Enescu, B., Hainzl, S., Ergintav, S., 2009. Afterslip and
795 viscoelastic relaxation following the 1999 M 7.4 Izmit earthquake from GPS measurements.
796 Geophys. J. Int. 178 (3), 1220–1237.
797 Wang, R., Schurr, B., Milkereit, C., Shao, Zh., Jin, M., 2011. An improved automatic
798 scheme for empirical baseline correction of digital strong-motion records. Bull. Seismol. Soc.
799 Am. 101 (5), 2029–2044. http://dx.doi.org/10.1785/0120110039.
800 Wang, K., Fialko, Y., 2014. Space geodetic observations and models of postseismic
801 deformation due to the 2005 M7.6 Kashmir (Pakistan) earthquake. J. Geophys. Res. 119, 7306–
802 7318.
803 Wang, R., Parolai, S., Ge, M., Jin, M., Walter, T.R., Zschau, J., 2012. The 2011 Mw 9.0
804 Tohoku Earthquake: comparison of GPS and strong-motion data. Bull. Seismol. Soc. Am.
805 http://dx.doi.org/10.1785/0120110264.

Wesnousky, S.G., Kumahara, Y., Chamlagain, D. & Neupane, P.C. 2019. Large Himalayan Frontal Thrust paleoearthquake at Khayarmara in Eastern Nepal. Journal of Asian Earth Sciences, https://doi.org/10.1016/j. jseaes.2019.01.008.

Wessel, P., Smith, W.H.F., 1995. New version of the Generic Mapping Tools released, EOS Trans. AGU, 76, 329.

Wheeler, J., Treloar, P.J. & Potts, G.J. 1995. Structural and metamorphic evolution of the Nanga Parbat syntaxis, Pakistan Himalayas, on the Indus gorge transect: the importance of early event. Geological Journal, 30, 349–371.

Wübbena, G., 1985. Software developments for geodetic positioning with GPS using TI4100 code and carrier measurements. Paper Presented at 1st International Symposium on Precise Positioning with the Global Positioning System, *Int. Assoc. of Geod*., Rockville, Md.

Yan, Y., V. Pinel, E. Trouve, E. Pathier, J. Perrin, P. Bascou, and F. Jouanne, 2013, Coseismic displacement field and slip distribution of the 2005 Kashmir earthquake from SAR amplitude image correlation and differential interferometry, Geophys. J. Int. 193, 29-46.

Zhao,W., Nelson, K.D., project INDEPTH Team, 1993. Deep seismic reflection evidence for continental underthrusting beneath southern Tibet. Nature 366, 55–559.

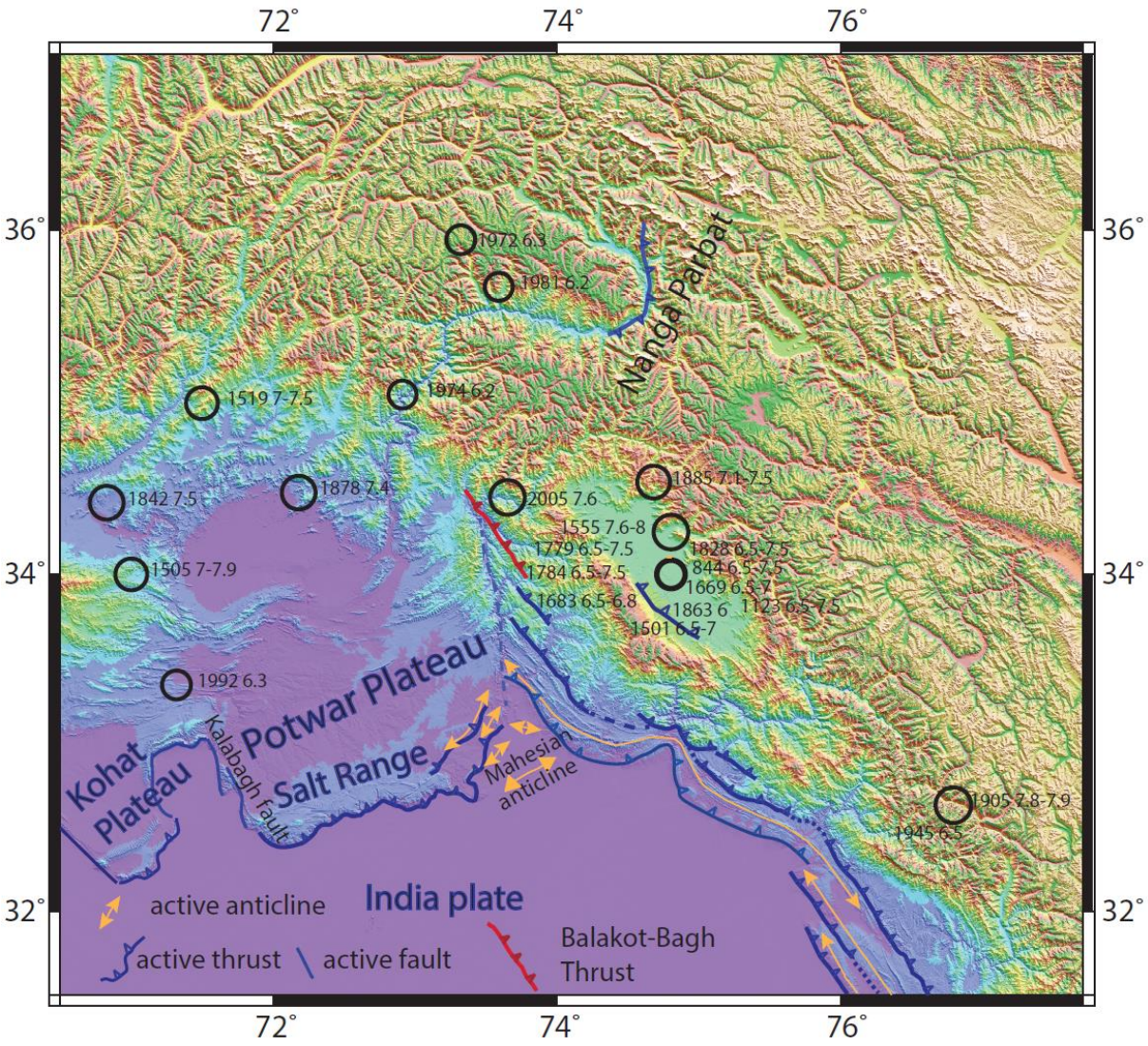

Figure 1. Historical seismicity in the northwestern Himalaya (Bilham, 2019) with the approximate locations and dates of large-magnitude earthquakes and the locations of active folds and faults.

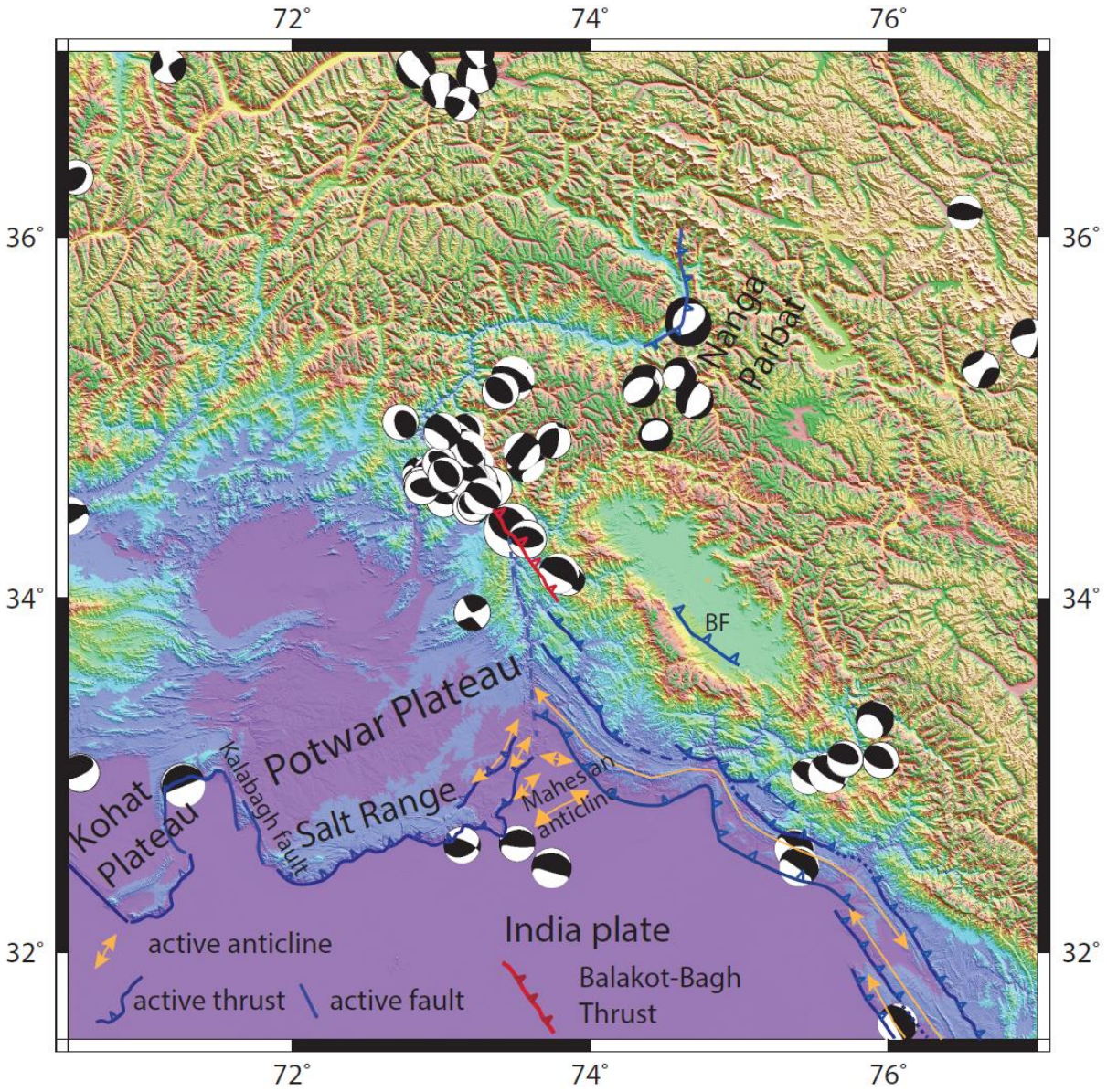

827

828 Figure 2. CMT focal mechanisms for the northwestern Himalaya (Dziewonski et al., 1981;
829 Ekström et al., 2012) and the locations of active folds and faults. BF Balapora fault.

830 .

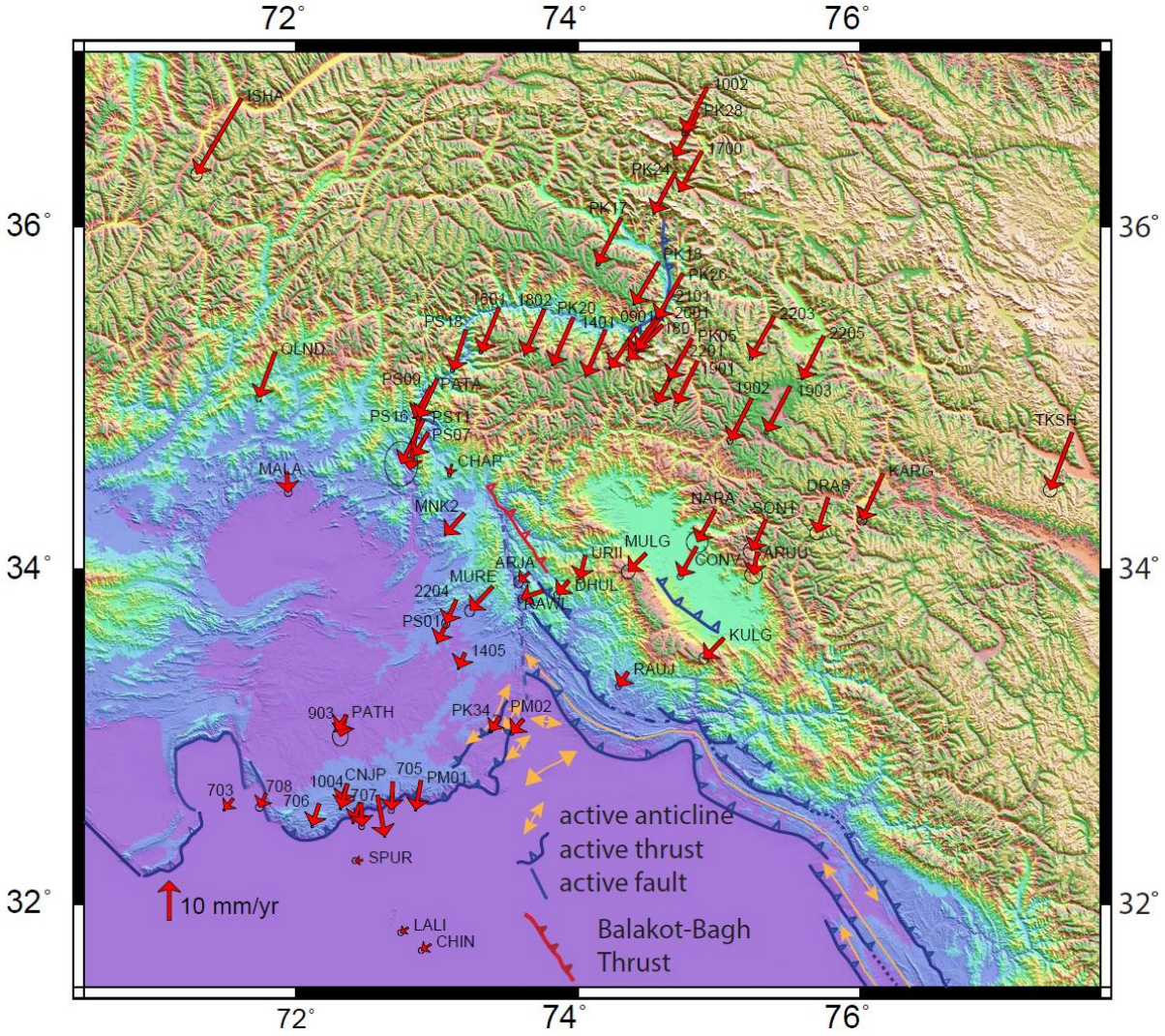

831

832 Figure 3. Velocities expressed in a reference plate with a fixed Indian plate and the locations
833 of active folds and faults.

834

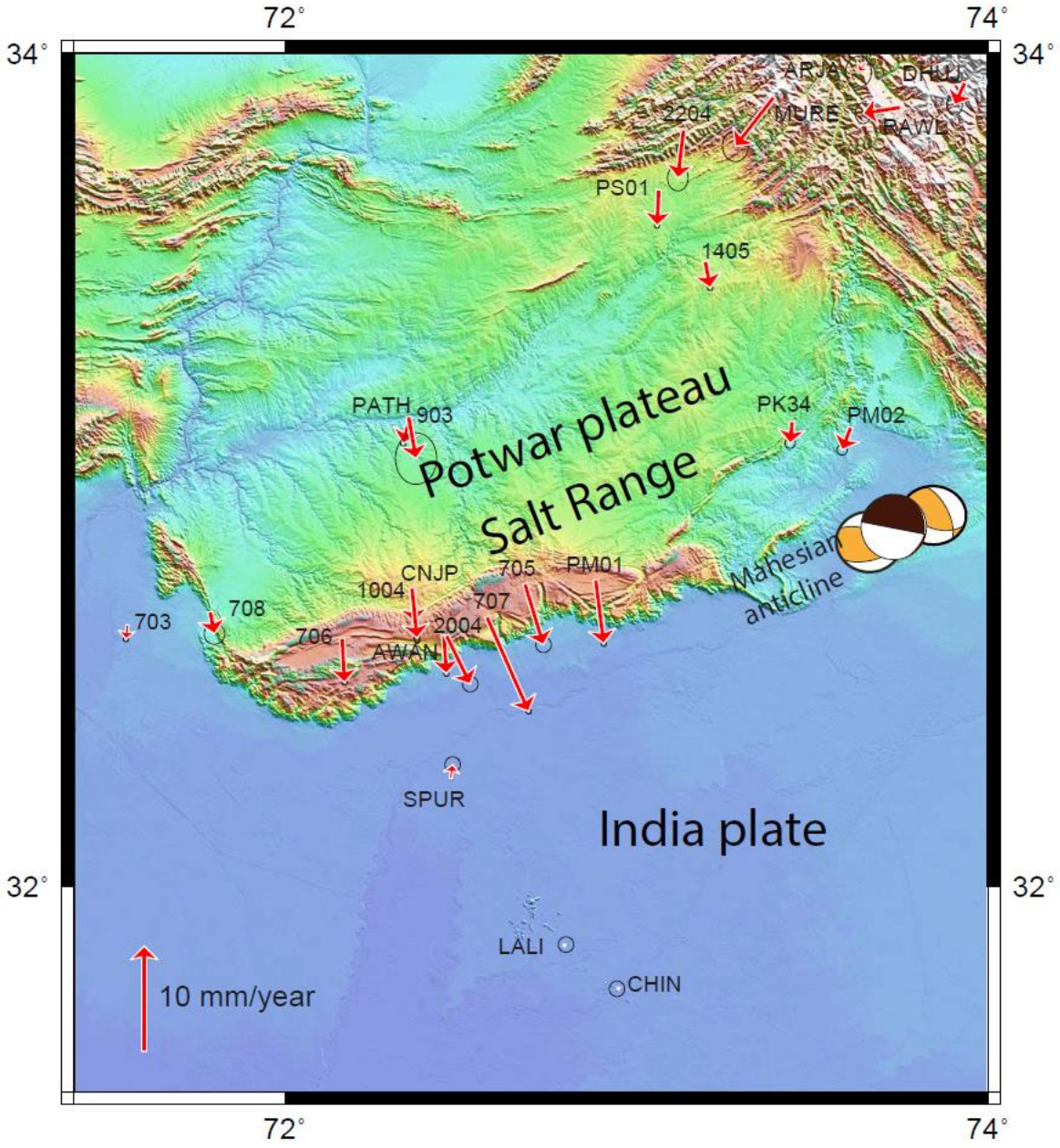

Figure 4. Velocities in the Potwar Plateau and Salt Range expressed in a reference frame modified to have average null velocities for points located in the foreland.

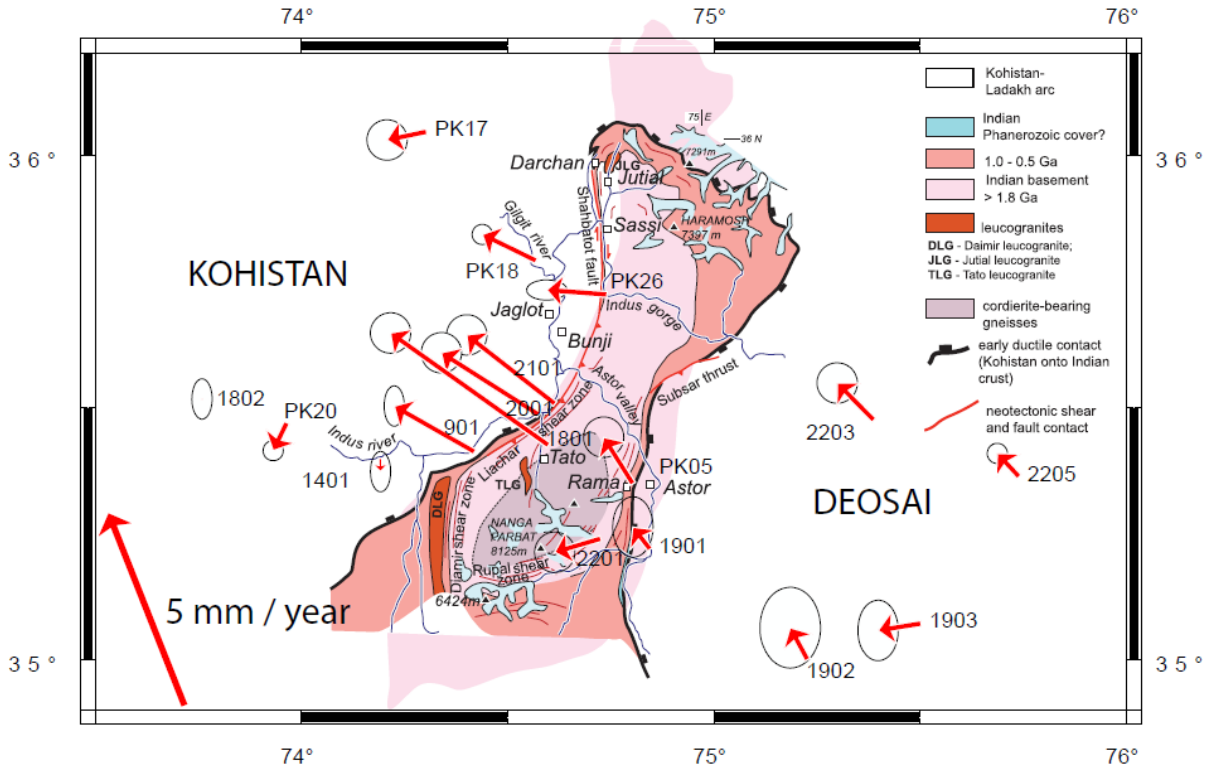

838

839 Figure 5. Velocities expressed relative to point 1802 located in the Kohistan Plateau illustrating
840 the existence of the ongoing deformation of the Nanga Parbat Massif characterized by active
841 westward thrusting along the Raikot-Liachar fault or Liachar shear zone.

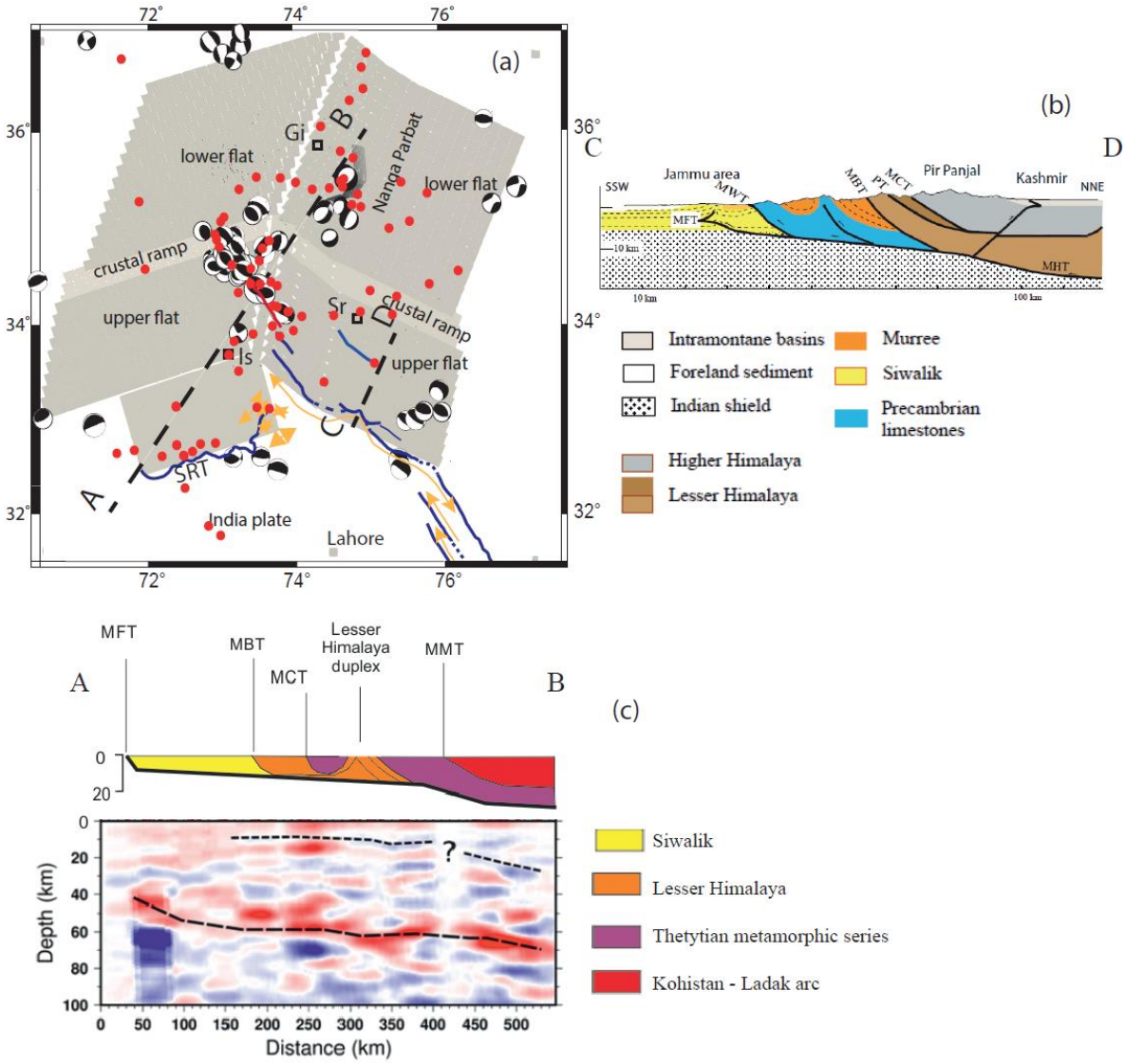

Figure 6. Geometry of the Main Himalayan Thrust used to estimate the slip distribution and coupling along this thrust and location of GNSS/GPS points used in this study.

.

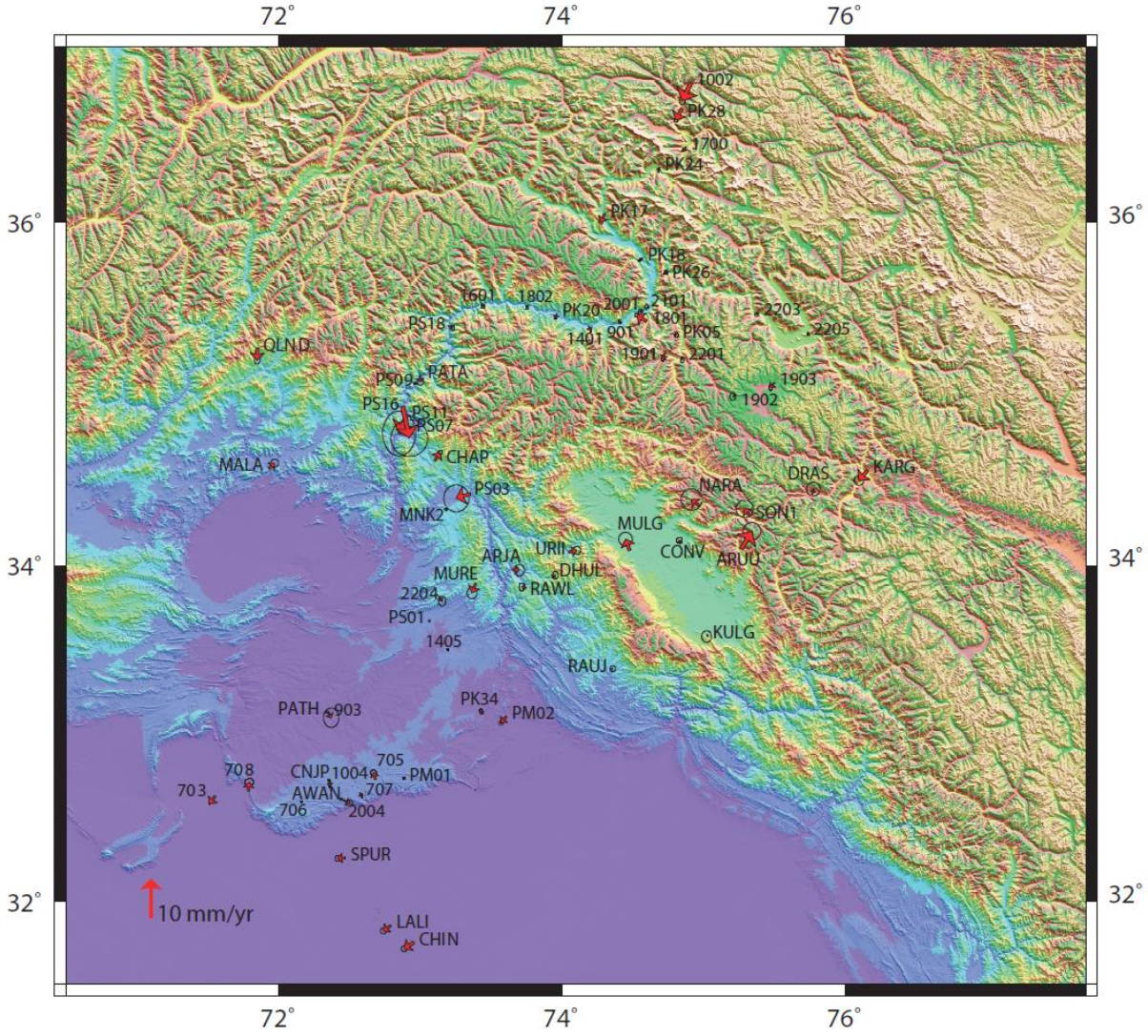

Figure 7. Residual velocities between the observed and simulated velocities in the India-fixed reference frame. Residuals are not significant except at points PS07, PS11 and PS16, at which contributions from the postseismic deformation following the 8 October 2005 Mw 7.6 Balakot-Bagh earthquake can be suspected.

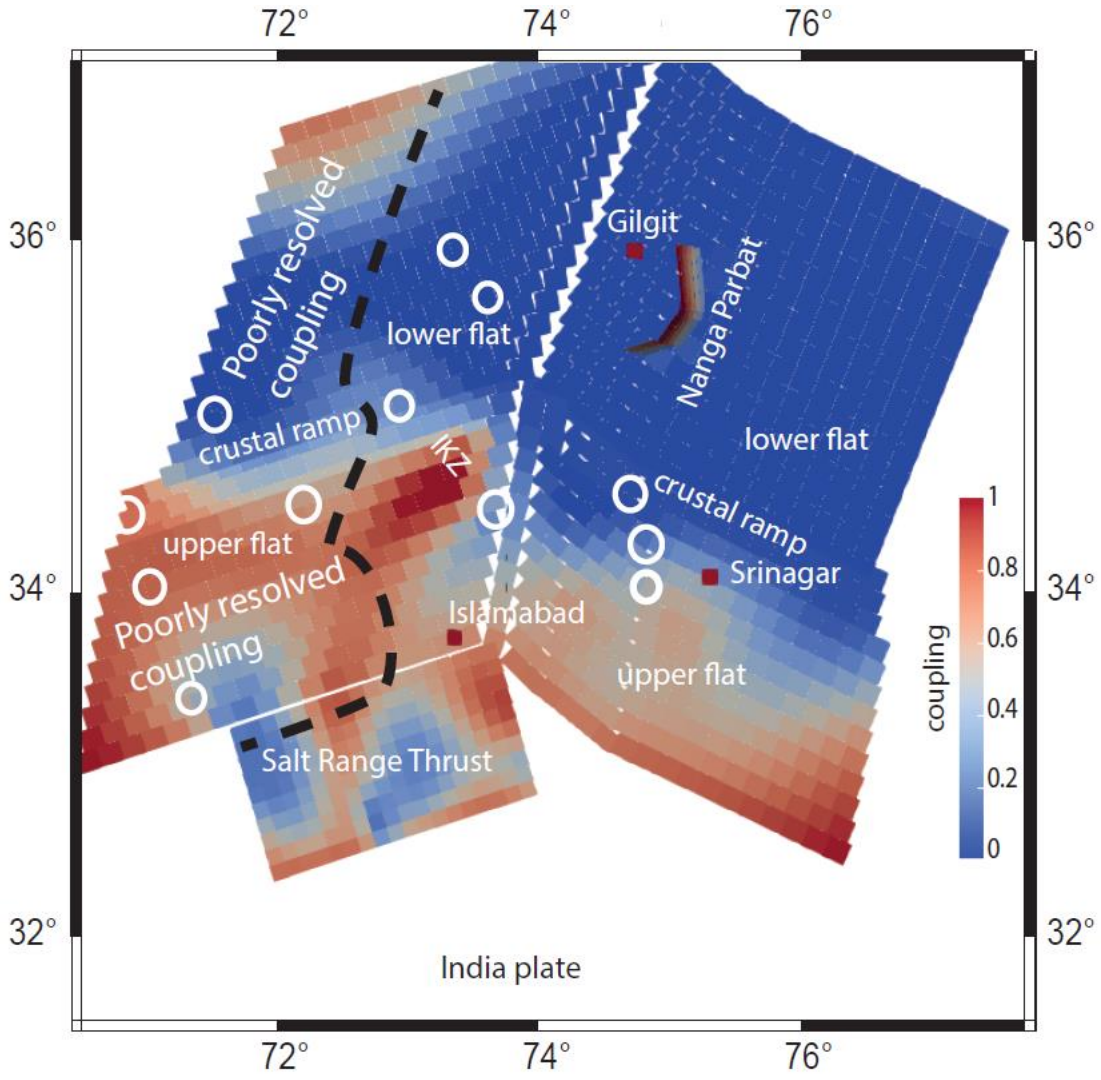

Figure 8. Map view of the coupling along the Main Himalayan Thrust with an upper flat that includes the Salt Range–Potwar Plateau Thrust, a crustal ramp, and a lower flat at depth. The changes in the geometry were determined using structural data, receiver function data and crustal cross sections. The approximate locations of historical earthquakes are indicated by white circles. The dashed line indicates the boundary of the domain where the coupling is poorly resolved from the domain where the coupling is well resolved as determined by the bootstrap method (Fig. 10).

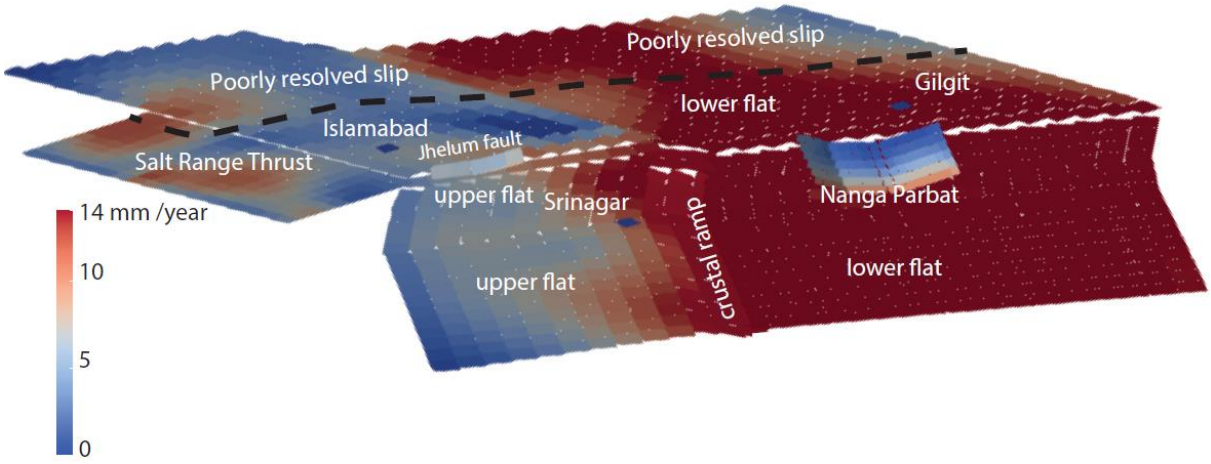

Figure 9. Slip distribution along the active faults of the northwestern Himalaya. The faults are the Main Himalayan Thrust, which has an upper flat that includes the Salt Range–Potwar Plateau Thrust, a crustal ramp, and a lower flat; the Jhelum strike-slip fault; and the Raikot-Liachar fault, which forms the western boundary of the Nanga Parbat Massif. The dashed line indicates the boundary of the domain where the coupling is poorly resolved from the domain where the coupling is well resolved as determined by the bootstrap method (Fig. 10).

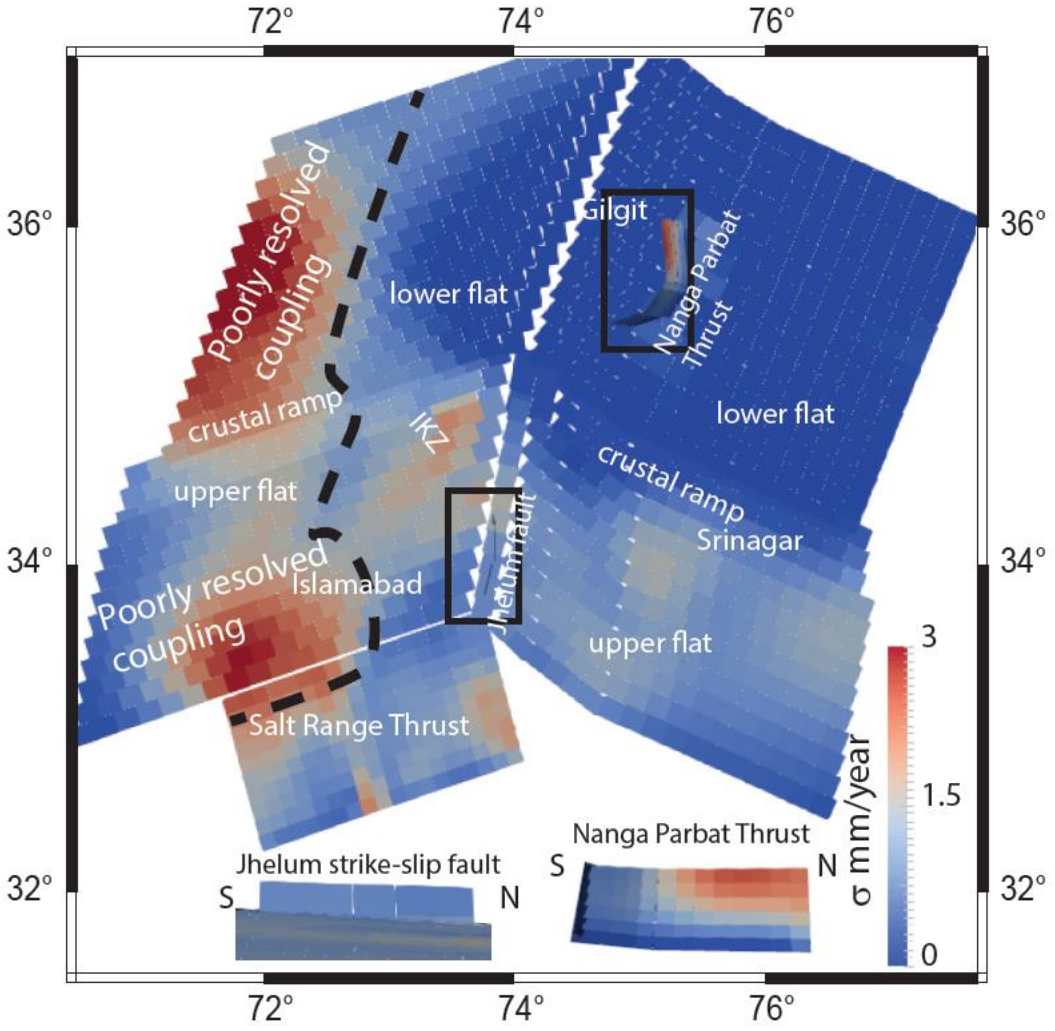

869

870 Figure 10. Simulation of the uncertainties on the slip on the patches using a bootstrap method.

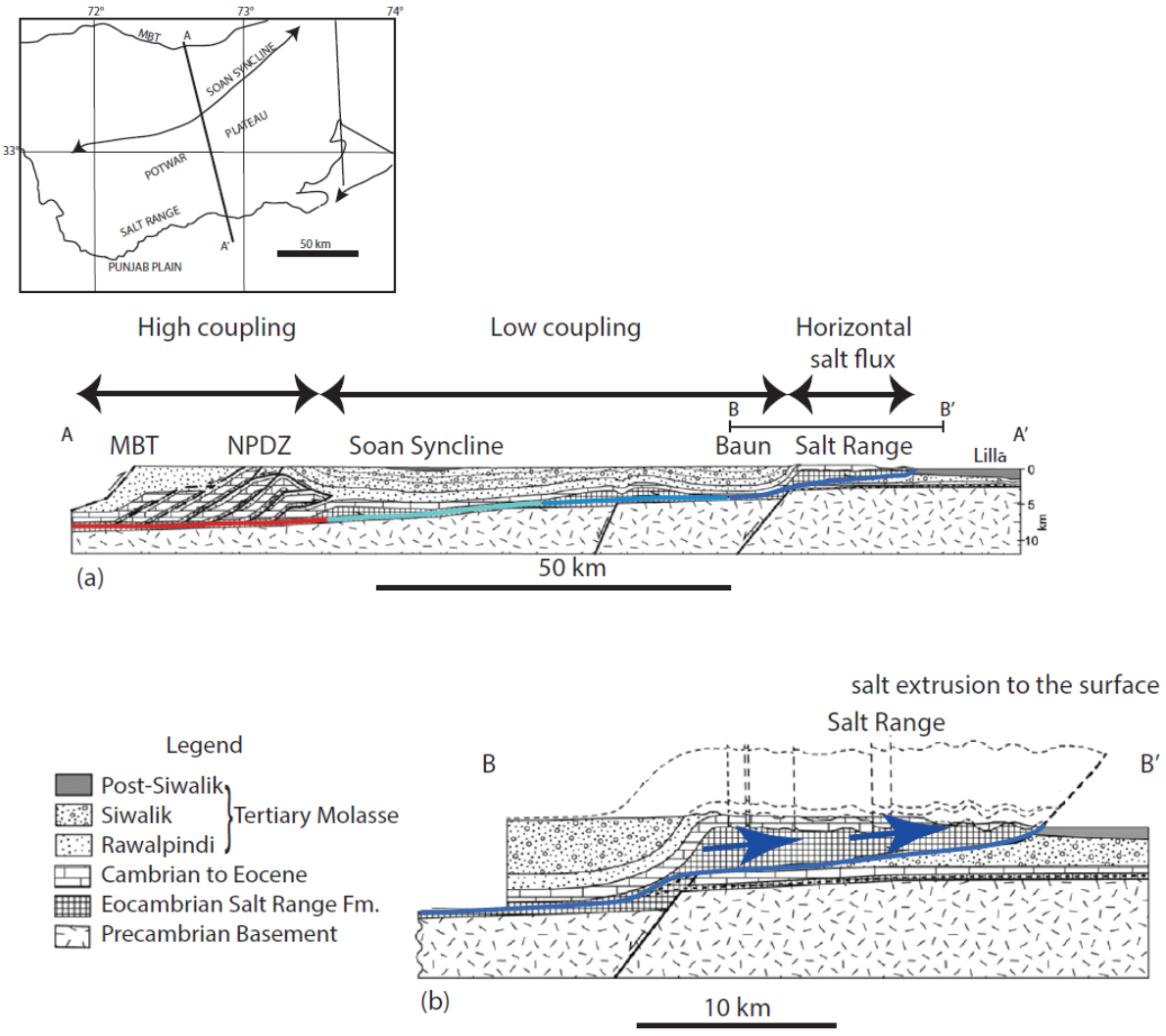

871

872 Figure 11. Cross section across the Potwar Basin and Salt Range (Faisal & Dixon, 2015) and
873 interpretation of the present-day deformation according to the existence or lack of massive salt
874 layers.

875

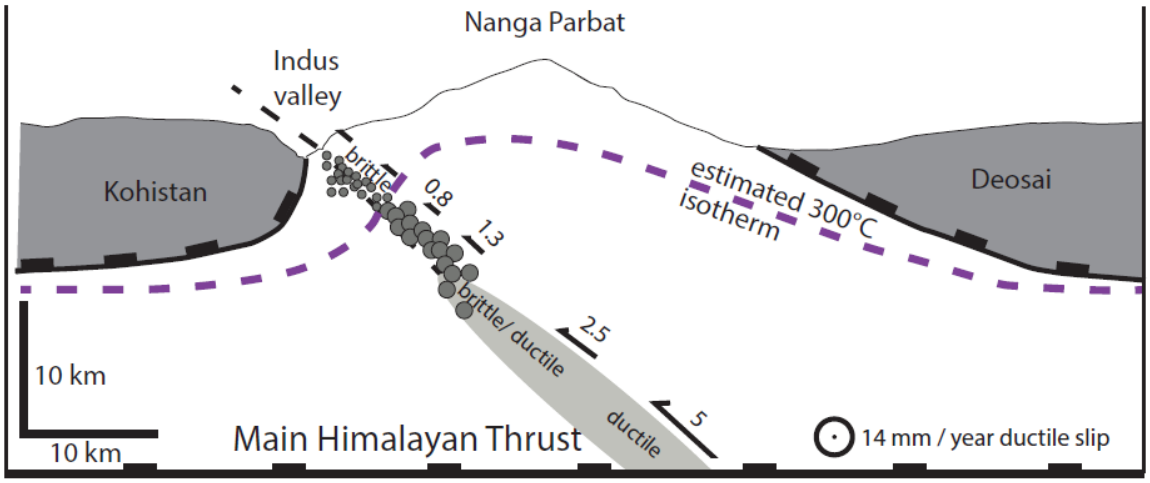

Figure 12. Crustal cross section across the Nanga Parbat Massif with estimation of 300°C isotherm (modified from Wheeler et al, 1995; Butler, 2018) with the distribution of microseismicity and estimated slip rates along the Liachar Thrust illustrating the evolution from ductile deformation at depth to brittle deformation with locked slip near the surface. Kohistan and Deosai are part of the Ladakh arc thrusted above the Himalayan basement.

			2001	2003	2005	2006	2007	2008	2009	2010	2011	2012	2017	2018	2019
703	71.5523	32.6328					3					2		3	
705	72.6833	32.7325					3					3			
706	72.1635	32.601					2								5
707	72.5748	32.6527					3								4
708	71.788	32.6648					3					3			
901	74.4199	35.4133					3				5				
903	72.3544	33.1267				3						4		22	
1002	74.9141	36.7953				3								3	
1004	72.3615	32.7189				3									3
1401	74.1908	35.4004				4								4	
1405	73.1966	33.5044				2						3		4	
1601	73.435	35.5264				3	2							3	
1700	74.8739	36.4307													
1801	74.5991	35.4265				4						4		4	
1802	73.7589	35.5181				2						3		4	
1901	74.8455	35.2196				2								3	
1902	75.2268	34.9996				3					3				
1903	75.5018	35.0722				5		3			4				
2001	74.5753	35.487				4					4			2	
2004	72.4526	32.609				2					2			3	
2101	74.6148	35.5084				4			2					5	
2201	74.7261	35.241				5			3		4				
2203	75.3878	35.4762				3					4				
2204	73.1349	33.8176				4					4				
2205	75.7399	35.3635				3		3			3			4	
ARJA	73.6533	33.9782													
ARUU	75.27	34.1													
AWAN	72.4595	32.6082		7		4	4	5							
CHAP	73.1058	34.6166	5		6	8				5					
CHIN	72.9542	31.7546		4	2		4	4							
CNJP	72.3618	32.7224					216	257	152						
CONV	74.84	34.13													
DHUL	73.9354	33.9301				8		6		6					
DRAS	75.77	34.42													

ISHA	71.6116	36.73					3		3		3				
LALI	72.7923	31.8564		4				4							
MALA	71.9335	34.572		5		6		7							
MNK2	73.1936	34.3288				258	145	29	32						
MURE	73.3915	33.8952				10		5							
PATA	72.9978	35.1121	1		5	7		5		5					
PATH	72.352	33.1339		2	9			6							
PK05	74.8036	35.3499				3					3			3	
PK17	74.3035	36.0458				6								4	
PK18	74.5692	35.7913				6			3		3			4	
PK20	73.9644	35.4713				3	2					4		4	
PK24	74.689	36.3124				4			5		3			5	
PK26	74.7409	35.7248				6		3						4	
PK28	74.8498	36.6486				4			1					6	
PK34	73.4439	33.1221				3	4					4			
PM01	72.8847	32.7421					3					3			
PM02	73.6106	33.1083					3							1	
PS01	73.0642	33.6749			10	44	36	4	10		34	7	3		
PS07	72.936	34.8023			5	9	2					2		3	
PS09	72.9543	35.0676				3	7							4	
PS11	72.9002	34.8768			3	7	2								
PS16	72.8763	34.932			2	7	2								
PS18	73.2013	35.3993				7	4							4	
QLND	71.8523	35.2718				6				5					
RAWL	73.7524	33.8708				9		4		5					
SPUR	72.4723	32.2631		5	4		9	5							

883 Table 1. Numbers of episodic GNSS measurements expressed as the number of 24-hour
884 sessions per year.

885

886

Point	Longitude	Latitude	Ve	Vn	σVe	σVn
703	71.552	32.633	-2.26	-2.79	0.1	0.1
705	72.683	32.733	-0.35	-7.26	0.3	0.3
706	72.163	32.601	-1.9	-5.65	0.1	0.1
707	72.575	32.653	1.86	-10.43	0.1	0.1
708	71.788	32.665	-1.71	-3.56	0.4	0.4
901	74.420	35.413	-6.93	-10.3	0.1	0.2
903	72.354	33.127	-2.7	-3.74	0.1	0.1
1002	74.914	36.795	-5.77	-11.37	0.3	0.4
1004	72.362	32.719	-1.83	-4.59	0.1	0.1
1401	74.191	35.400	-4.97	-11.73	0.1	0.2
1405	73.197	33.504	-1.65	-3.96	0.1	0.1
1601	73.435	35.526	-4.51	-11.18	0.2	0.2
1700	74.874	36.431	-5.69	-10.26	0.1	0.1
1801	74.599	35.426	-8.81	-8.69	0.2	0.2
1802	73.759	35.518	-4.98	-11.41	0.1	0.2
1901	74.846	35.220	-5.4	-10.87	0.2	0.3
1902	75.227	35.000	-5.4	-10.63	0.3	0.4
1903	75.502	35.072	-6.02	-11.58	0.2	0.3
2001	74.575	35.487	-7.34	-9.91	0.2	0.2
2004	72.453	32.609	-1.88	-5.13	0.1	0.1
2101	74.615	35.508	-7.12	-9.74	0.2	0.2
2201	74.726	35.241	-6.1	-11.74	0.2	0.2
2203	75.388	35.476	-5.87	-10.51	0.2	0.2
2204	73.135	33.818	-2.66	-6.03	0.4	0.5
2205	75.740	35.364	-5.51	-10.84	0.1	0.1
ARJA	73.653	33.978	-2.8	-2.36	0.5	0.6
ARUU	*75.270*	*34.100*	*-0.99*	*-5.81*	*0.9*	*0.9*
AWAN	72.460	32.608	0.16	-6.09	0.3	0.3

CHAP	73.106	34.617	-0.69	-2.67	0.2	0.2
CHIN	72.954	31.755	-2.41	-1.54	0.3	0.3
CNJP	72.362	32.722	-1.63	-6.22	0.1	0.2
CONV	*74.840*	*34.130*	*-4.23*	*-7.55*	*0.3*	*0.3*
DHUL	*73.935*	*33.930*	*-3.1*	*-3.58*	*0.3*	*0.4*
DRAS	*75.770*	*34.420*	*-2.88*	*-8.99*	*0.7*	*0.7*
ISHA	71.612	36.730	-11.37	-19.18	0.6	0.7
KARG	*76.160*	*34.560*	*-5.33*	*-11.85*	*0.5*	*0.5*
KULG	*75.030*	*33.590*	*-5*	*-5.18*	*0.5*	*0.6*
LALI	72.792	31.856	-1.85	-1.31	0.3	0.3
MALA	71.933	34.572	0.33	-5.29	0.4	0.4
MNK2	73.194	34.329	-4.91	-5.44	0.1	0.1
MULG	*74.480*	*34.090*	*-4.53*	*-4.59*	*0.7*	*0.7*
MURE	73.392	33.895	-5.76	-6.1	0.5	0.6
NARA	*74.970*	*34.350*	*-4.55*	*-8.27*	*1.1*	*1.1*
PATA	72.998	35.112	-4.63	-9.72	0.3	0.3
PATH	72.352	33.134	-1.4	-5.45	0.8	1
PK05	74.804	35.350	-5.69	-10.28	0.2	0.2
PK17	74.303	36.046	-5.94	-11.61	0.2	0.2
PK18	74.569	35.791	-6.29	-10.77	0.1	0.1
PK20	73.964	35.471	-5.31	-12.09	0.1	0.1
PK24	74.689	36.312	-5.54	-10.43	0.1	0.2
PK26	74.741	35.725	-6.44	-11.3	0.2	0.1
PK28	74.850	36.649	-5.91	-11.13	0.2	0.2
PK34	73.444	33.122	-2.31	-3.52	0.2	0.2
PM01	72.885	32.742	-1.35	-7.53	0.1	0.1
PM02	73.611	33.108	-2.95	-3.61	0.2	0.2
PS01	73.064	33.675	-2.28	-4.85	0.1	0.1
PS03	73.356	34.422	-8.73	-8.14	1.3	1.4
PS07	72.936	34.802	-3.59	-5.92	0.1	0.1
PS09	72.954	35.068	-4.24	-7.85	0.2	0.1
PS11	72.900	34.877	-5.58	-11.21	1.7	2.3
PS16	72.876	34.932	-2.6	-15.08	1.9	1.9
PS18	73.201	35.399	-3.25	-10.24	0.2	0.2
QLND	*71.852*	*35.272*	*-4.22*	*-11.64*	*0.3*	*0.4*
RAUJ	74.350	33.390	-2.39	-3.77	0.3	0.3
RAWL	*73.752*	*33.871*	*-5.68*	*-2.01*	*0.3*	*0.4*
SON1	*75.330*	*34.290*	*-3.51*	*-7.92*	*0.9*	*0.9*
SPUR	*72.472*	*32.263*	*-1.94*	*-0.15*	*0.3*	*0.3*
TKSH	*77.500*	*34.800*	*-5.56*	*-14.53*	*0.7*	*0.7*
URII	*74.050*	*34.080*	*-1.4*	*-6.02*	*0.4*	*0.4*

Table 2. Velocities expressed in the India-fixed reference frame.

	Positions of points describing the location of the upper boundary of the fault		depth of upper boundary	dip	width	patch size	max slip	Rake
	Latitude	longitude						
Salt Range Thrust	32.3145	71.8659	2	5	75	10	14 mm/year	-120° to -30°
	32.8328	73.6549						
Upper Flat of MHT	32.8705	70.5156	10	2	145	15	14 mm/year	-120° to -30°
	33.6806	73.3116						
	33.4494	73.6044						
	33.0962	74.1431						
	32.4970	75.7067						
Crustal ramp of MHT	34.1176	70.8103	14.8	15	45	15	14 mm/year	-120° to -30°
	34.8664	73.4472						
	34.7894	73.7808						
	34.6790	73.9128						
	34.4252	74.3045						
	33.7983	75.9366						
Lower flat of MHT	34.5072	71.0966	26	1	275	15	14 mm/year	-120° to -30°
	35.1581	73.4065						
	35.1879	73.6076						
	34.8072	74.1677						
	34.6004	74.5775						
	34.0965	75.8894						
Nanga Parbat Thrust	36.0408	74.6099	0	40	30	5	10 mm/year	-110° to -50°
	35.7466	74.6466						
	35.6539	74.6502						
Jhelum fault	34.3616	73.4654	0	80	15	10	8 mm/year	-180° to 180°
	34.0971	73.4818						
	33.8841	73.4187						

Table 3. Characteristics of the faults considered to establish our coupling and slip model along active faults in the northwestern Himalayas.